


Review

Recent Advances in the Use of Controlled Nanocatalysts in Methane Conversion Reactions

Felipe Anchieta e Silva and Thenner Silva Rodrigues * 

Nanotechnology Engineering Program, Alberto Luiz Coimbra Institute for Graduate Studies and Research in Engineering, Federal University of Rio de Janeiro, Av. Horácio Macedo, 2030, Rio de Janeiro 21941-972, RJ, Brazil; felipe.anchieta@coppe.ufrj.br

* Correspondence: thenner@pent.coppe.ufrj.br

Abstract: This study investigates the utilization of controlled nanocatalysts in methane conversion reactions, addressing the pressing need for the efficient utilization of methane as a feedstock for valuable chemicals and clean energy. The methods employed include a comprehensive review of recent advancements in nanocatalyst synthesis, characterization, and application, as well as the critical analysis of underlying mechanisms and controversies in methane activation and transformation. The main findings reveal significant progress in the design and synthesis of controlled nanocatalysts, enabling enhanced activity, selectivity, and stability in methane conversion reactions. Moreover, the study highlights the importance of resolving controversies surrounding metal–support interactions for rational catalyst design. Overall, the study underscores the pivotal role of nanotechnology in shaping the future of methane utilization and sustainable energy production, providing valuable insights for guiding future research directions and technological developments in this field.

Keywords: methane conversion; controlled nanomaterials; nanocatalysis



Citation: e Silva, F.A.; Rodrigues, T.S. Recent Advances in the Use of Controlled Nanocatalysts in Methane Conversion Reactions. *Methane* **2024**, *3*, 359–379. <https://doi.org/10.3390/methane3020020>

Academic Editor: Lubomira Tosheva

Received: 27 February 2024

Revised: 17 April 2024

Accepted: 23 May 2024

Published: 11 June 2024



Copyright: © 2024 by the authors. Licensee MDPI, Basel, Switzerland. This article is an open access article distributed under the terms and conditions of the Creative Commons Attribution (CC BY) license (<https://creativecommons.org/licenses/by/4.0/>).

1. Introduction

The quest for sustainable energy sources has spurred immense interest in methane conversion reactions, given the abundance of methane and its potential as a feedstock for valuable chemicals and clean energy [1]. In this context, nanotechnology offers unprecedented opportunities to revolutionize catalysis, enabling precise control over reaction pathways and enhancing catalytic performance. The utilization of controlled nanocatalysts represents a paradigm shift in catalytic processes, offering enhanced activity, selectivity, and stability compared to conventional catalysts [2,3]. Methane, as the main constituent of natural gas, holds tremendous promise as a feedstock to produce value-added chemicals and clean fuels. However, its inert C-H bonds pose a significant challenge for activation and conversion under mild conditions. Traditional catalysts often suffer from low activity, poor selectivity, and rapid deactivation, hindering the development of efficient methane conversion processes [4,5]. The emergence of controlled nanocatalysts has opened new avenues for addressing these challenges, offering unprecedented control over catalyst structure, composition, and surface properties, as depicted in Figure 1.

In recent years, significant progress has been made in the design, synthesis, and application of controlled nanocatalysts for methane conversion reactions [2,4]. Fundamental studies have elucidated the underlying mechanisms governing methane activation and subsequent transformations of nanostructured catalysts [3]. Key advancements include the development of novel synthesis techniques, such as colloidal chemistry, atomic layer deposition, and template-assisted methods, enabling precise control over nanoparticle size, shape, and morphology [3,6]. Moreover, advances in characterization techniques, such as in situ spectroscopy and microscopy, have provided invaluable insights into the dynamic behavior of nanocatalysts under reaction conditions [6]. Despite significant progress, several controversies and diverging hypotheses persist in the field of methane conversion

catalysis. One such debate revolves around the role of metal–support interactions in determining the catalytic activity and selectivity of supported nanocatalysts. While some studies emphasize the importance of strong metal–support interactions for stabilizing active metal nanoparticles and facilitating methane activation, others suggest that excessive metal–support interactions may lead to catalyst encapsulation and deactivation. Resolving these controversies is essential for the rational design of efficient nanocatalysts to be used for methane conversion reactions [7,8].

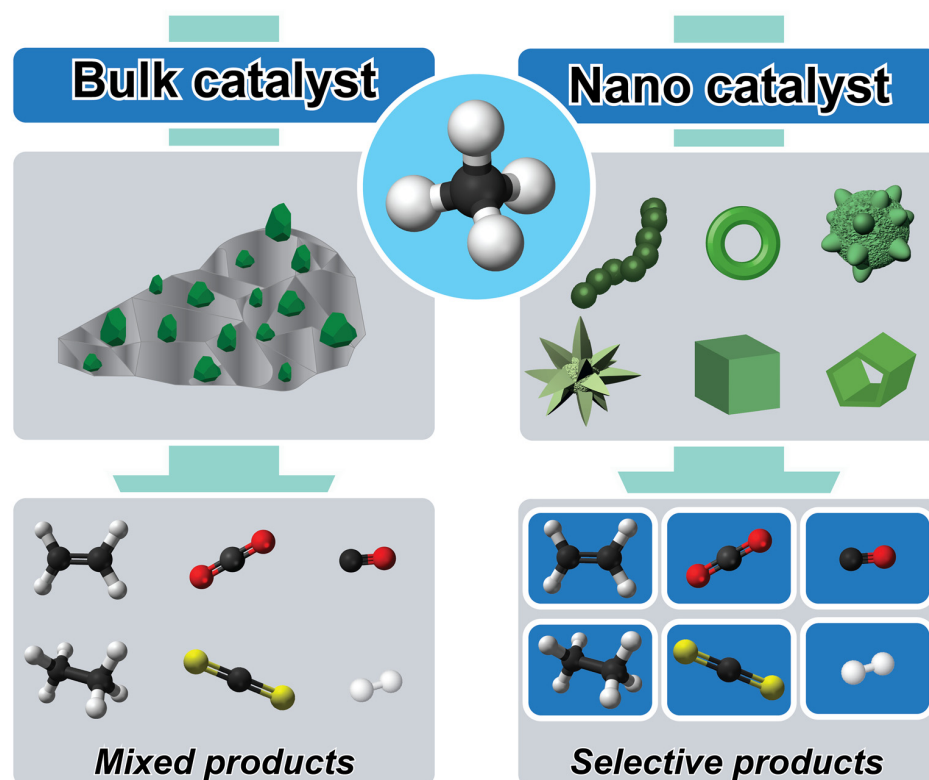


Figure 1. Schematic illustration of the catalytic conversion of methane over bulk catalysts and nanocatalysts to produce mixed products and selective products, respectively.

In this review, we aim to provide a comprehensive overview of the recent advances in the use of controlled nanocatalysts for methane conversion reactions. We will critically analyze the underlying principles governing methane activation, hydrocarbon transformation, and product selectivity on nanostructured catalysts. Furthermore, we will discuss key challenges and opportunities in the field, highlighting emerging strategies for enhancing catalytic performance and sustainability. By synthesizing insights from a diverse range of studies, this review aims to guide future research directions and inspire innovative approaches towards efficient methane utilization. The main aim of this work is to elucidate the pivotal role of controlled nanocatalysts in enabling efficient methane conversion reactions. By highlighting recent advancements and addressing existing controversies, we seek to provide a holistic understanding of the underlying principles governing catalytic processes on the nanoscale. Through a critical analysis of key publications and experimental findings, we aim to identify promising avenues for further research and development in this rapidly evolving field. Ultimately, this review underscores the significance of nanotechnology in shaping the future of methane utilization and sustainable energy production. In conclusion, the integration of controlled nanocatalysts holds immense potential for transforming methane into a versatile platform for the synthesis of chemicals, fuels, and materials. By harnessing the unique properties of nanomaterials and leveraging the synergistic effects at the nanoscale, researchers can unlock new pathways towards a greener and more sustainable energy future.

2. Controlled Nanocatalysts: A Comprehensive Overview

Nanotechnology has emerged as a powerful tool in the realm of catalysis, offering unprecedented control over catalyst properties and enabling the development of highly efficient and selective catalysts for various chemical transformations. In the context of methane conversion reactions, the utilization of controlled nanocatalysts represents a paradigm shift, promising to address the longstanding challenges associated with the activation and transformation of this abundant but inert hydrocarbon [9]. This section provides a comprehensive overview of the fundamentals of controlled nanocatalysts, highlighting their unique properties and advantages in catalyzing methane conversion reactions.

Controlled nanocatalysts refer to catalysts comprising nanoscale materials with precisely engineered structures, compositions, and surface properties tailored to catalyze specific reactions with high efficiency and selectivity [10]. The nanoscale dimensions of these catalysts impart unique physicochemical properties, such as a high surface area-to-volume ratio, size-dependent electronic properties, and enhanced surface reactivity, which are instrumental in facilitating catalytic processes [11,12]. The controlled synthesis of nanocatalysts allows for the precise manipulation of these properties, enabling the design of catalysts which are optimized for desired reaction pathways and product distributions.

A variety of synthesis methods have been developed for the preparation of controlled nanocatalysts, each offering distinct advantages in terms of control over catalyst morphology, composition, and structure [13], as depicted in Figure 2. Common techniques include wet-chemical methods such as sol-gel synthesis, co-precipitation, and hydrothermal synthesis, which afford control over nanoparticle size, shape, and crystallinity through the precise control of reaction conditions and precursor chemistry [14–16]. Other approaches, such as chemical vapor deposition, physical vapor deposition, and template-assisted synthesis, enable the fabrication of nanocatalysts with well-defined nanostructures, including nanowires, nanotubes, and porous materials [17,18]. Recent advancements in colloidal chemistry, atomic layer deposition, and self-assembly techniques have further expanded the toolbox for synthesizing controlled nanocatalysts with tailored properties for methane conversion applications [11].

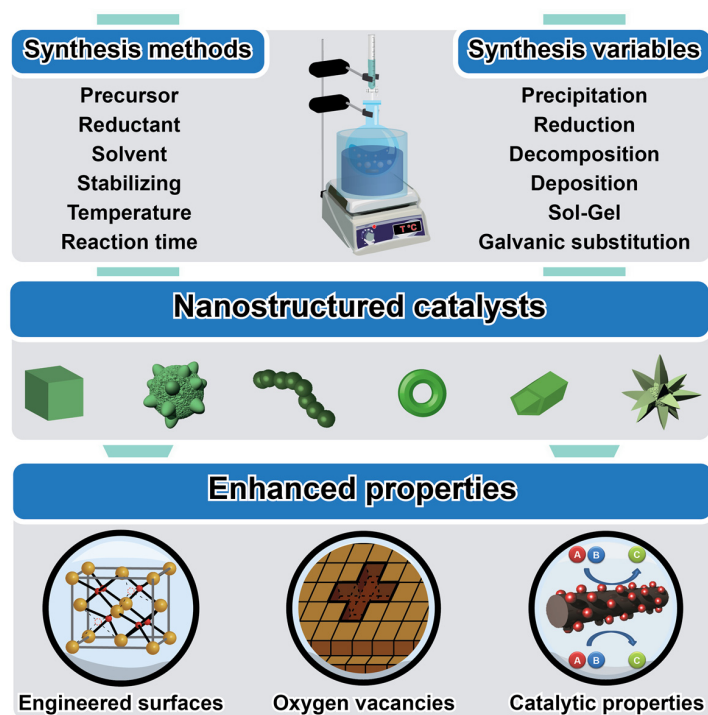


Figure 2. Schematic illustration outlining the fundamentals of controlled nanocatalysts, elucidating the main synthesis methods and their variables, as well as the improved properties.

The tailored design of nanocatalysts for methane conversion applications requires the careful consideration of several key factors, including catalyst composition, structure, and surface properties [19,20]. Noble metals such as palladium, platinum, and rhodium are commonly employed as active components due to their high catalytic activity and selectivity towards methane activation and subsequent transformations [21,22]. The choice of support material is critical in stabilizing and dispersing active metal nanoparticles, with oxides such as alumina, silica, and ceria being frequently used to provide a high surface area and thermal stability [23,24]. Furthermore, the introduction of promoters, dopants, or modifiers can tailor the electronic and chemical properties of nanocatalysts to enhance catalytic performance and selectivity towards desired products [24,25]. Rational catalyst design strategies, informed by theoretical modeling and experimental insights, enable the optimization of nanocatalysts for specific methane conversion reactions, including methane combustion, partial oxidation, steam reforming, and dry reforming [26–28].

Significant progress has been made in recent years towards the development and application of controlled nanocatalysts for methane conversion reactions. Fundamental studies have elucidated the mechanisms of methane activation and transformation on nanoscale catalysts, providing insights into key factors governing catalytic performance [29,30]. Experimental and computational approaches have been employed to characterize the structure–activity relationships of nanocatalysts and identify the optimal catalyst formulations for enhanced methane conversion efficiency and selectivity [31,32]. Moreover, advances in *in situ* and *operando* characterization techniques have enabled the real-time monitoring of catalyst dynamics under reaction conditions, facilitating the rational design of nanocatalysts with improved stability and performance [33].

In conclusion, controlled nanocatalysts offer immense potential for advancing methane conversion reactions through their unique properties and tailored design. By harnessing the principles of nanotechnology, researchers can overcome the longstanding challenges associated with methane activation and transformation, paving the way for more efficient and sustainable processes. The synthesis methods and design strategies outlined in this section provide a roadmap for the rational development of nanocatalysts optimized for methane conversion applications. Moving forward, interdisciplinary collaborations and continued innovation are essential to unlock the full potential of controlled nanocatalysts and realize the promise of methane as a renewable feedstock to produce fuels and chemicals.

3. Methane Activation Strategies

Recent strategies for methane activation using controlled nanocatalysts have been employed to overcome the barriers associated with heterogeneous catalysts. The enhanced surface properties of controlled nanostructures lead to a higher number of active and more reactive sites, facilitating the reaction with methane and yielding more valuable products [5].

In Figure 3, methane activation is depicted as being dependent on the interaction between methane and the surface, occurring through either a radical or surface-stabilizer pathway. The methane conversion process involves the initial breaking of the C-H bond [30]. In Figure 3A, a homolytic radical mechanism is illustrated. This mechanism proceeds through hydrogen abstraction via active oxygen species in the M-O active site, resulting in the formation of a hydrogen atom adsorbed on the catalyst surface (M-OH) and a free methyl radical ($^{\bullet}\text{CH}_3$) with sp^2 hybridization and a trigonal planar geometry [30,34,35]. The $^{\bullet}\text{CH}_3$ radical does not form M-C bonds with active sites, and the $^{\bullet}\text{H}$ exhibits a weak interaction forming OH groups. Additionally, a one-electron redox process occurs, leading to the oxidation of the carbon center from the -4 state to the -3 state and the corresponding reduction of the active sites [29,30]. This process requires strong oxidants, such as H_2O_2 and N_2O , and high metal oxidation states to form electron-deficient species, such as O^- and O^{2-} , thereby promoting the homolytic dissociation of C-H bonds [5,29,30,34,36]. The enhanced properties, such as oxygen vacancies, promoted in MgO , CeO_2 , TiO_2 , and TbO_x contribute to a stronger ability to activate methane due to the easily reducible surface [29,30].

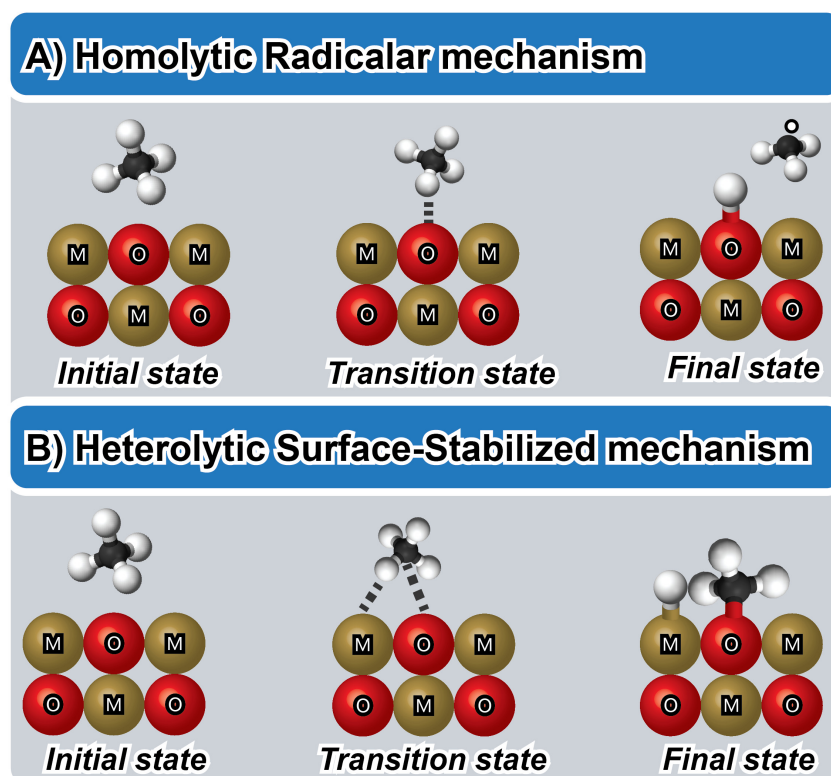


Figure 3. Schematic illustration of the methane activation strategies via the homolytic radical mechanism (A) and heterolytic surface-stabilized mechanism (B) [5].

In Figure 3B, a heterolytic surface-stabilized mechanism is illustrated, utilizing surface Lewis acid-base pairs (M-X) as active sites to dissociate adsorbed methane and produce CH_3^- and H^+ [5,30]. The metal atom stabilizes the sp^3 -hybridized methyl group in a tetrahedral geometry via the σ -bond [5,29]. Simultaneously, hydrogen protons are accepted through the X atom, including surface nucleophilic oxygen species, surface metals, and ligands. The M-O active site with a low metal oxidation state is more favorable for the formation of electron-saturated oxygen atoms (O^{2-}) to accept hydrogen protons and promote the heterolytic mechanism [5,29]. Latimer et al., through DFT calculations, estimate that the maximum distance for methyl surface-stabilized requires a distance of 2\AA [5]. This can be rationalized through arguing that the heterolytic bond cleavage favored by acid-base pairs is governed by more long-range ionic interactions than homolytic cleavage, which occurs when no acid-base pair is present to polarize the bond. Catalysts with specific surface functionalities play a crucial role in stabilizing methane molecules, lowering activation energy, promoting selective transformations, and minimizing unwanted by-products [5,29,30,34,36].

Interestingly, the engineered surface in controlled nanomaterials is fundamental for optimizing methane activation surface defects such as oxygen vacancies, acidity, and basicity. By controlling synthetic parameters, including size, morphology, structure, and composition, it is possible to regulate the electronic and surface properties of nanomaterials [37,38]. Reducing the size of nanomaterials influences the surface-to-volume ratio, lattice parameters, and changes the surface energy of the metal oxide crystal [39–41]. This reduction in lattice parameters alters the geometric and electronic structure of the metal oxide by modifying the distance between atoms in the crystalline lattice. With increased surface energy, the surface bonds weaken, favoring the output of oxygen atoms that cannot be accommodated, leaving excess electrons in the material to form O_2 and H_2O [42]. Additionally, morphology is crucial because nanomaterials of different dimensions exhibit specific quantum confinement effects on electronic properties. For example, bulk materials, such as 3D materials, display lower surface activity, whereas nanosheets, nanofilms

(2D materials), nanowires, nanotubes (1D materials), quantum dots, and small nanoparticles (0D materials) exhibit higher levels of activity [43]. Densified and hollow structures exhibit different electronic properties; a nanoshell can display a thin layer thickness, lattice structure contraction, and intensified oxygen vacancies. The composition of nanomaterials controls the introduction of a positive or negative charge, regulating the surface activity, acidity, basicity, and electronic charge [12,42,44,45]. Additionally, modifications in the electronic and surface structure can control the reducibility of nanomaterials, directly affecting the mechanism of methane activation via a nanomaterial, whether it acts as a carbon acceptor or not.

4. Reaction Mechanisms and Kinetics of Methane in Sustainable Energy Production

Understanding the reaction mechanism of methane conversion is essential to design a nanocatalyst with the specific physicochemical, surface, and electronic properties required to transform methane into more valuable products such as methanol (CH_3OH) and C^{2+} hydrocarbons [46–51]. This section will return to some relevant catalytic reaction mechanisms in methane conversion to highlight the catalyst properties, such as oxygen vacancies, acidic and basic sites, and the electronic characteristics of the active sites. However, methane conversion is a huge topic that has been widely investigated for over a century, influencing numerous books which have deep approached each specific topic. We recommend some recent review articles to delve deeper into each catalytic reaction, such as the nonoxidative conversion of methane [52–58], methane oxidation [4,53,59–62], methane-to-methanol [49,53,59,63–66], the oxidative coupling of methane [47,50,53,67–70], methane steam reforming [25,53,60,71–75], the dry reforming of methane [4,24,25,28,32,53,60,73,74,76–83], electrocatalysis [84–92], and photocatalysis [9,11,67,93–99].

Figure 4 presents a diagram depicting two pathways for methane conversion. Activating methane and oxidizing it usually requires highly reactive conditions or aggressive reactants due to the significant energy barriers involved [46]. Transition metal-based catalysts have shown effectiveness in surmounting these barriers by efficiently activating the C-H bond [46,49,50,100]. For instance, the pathway from methane to methanol has been extensively researched and involves various forms of transition metals in their atomic and oxide states. This system offers advantages like low oxidation energy barriers and weak methanol adsorption onto active sites [46,49,100].

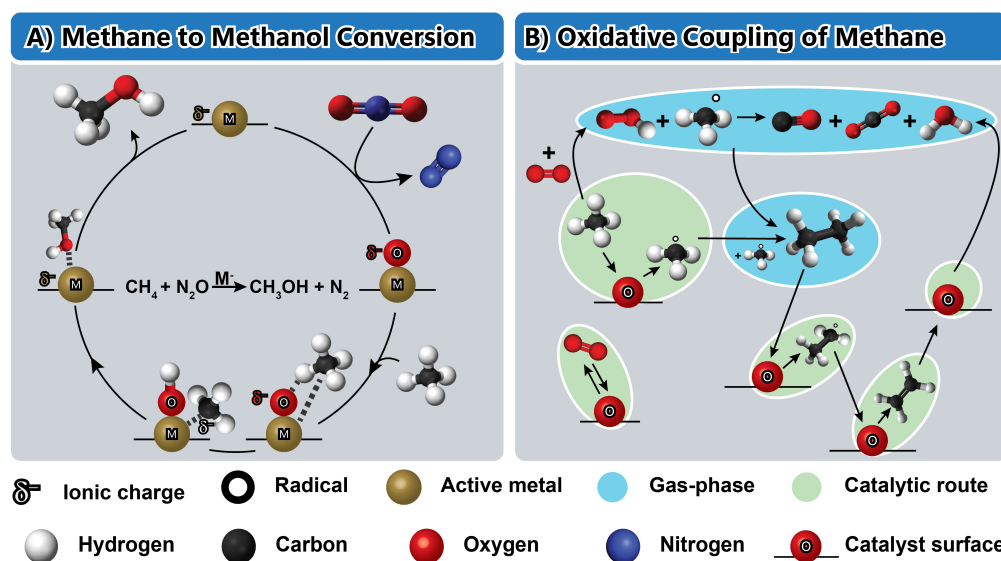
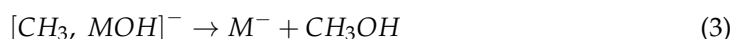
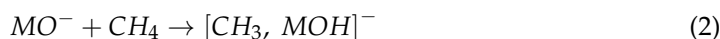


Figure 4. Schematic illustration of the catalytic reaction mechanism of the methane-to-methanol conversion (A) and oxidative coupling of methane (B). The scheme (A) is reproduced with permission from [100], American Chemical Society Publications, 2021. The scheme (B) is reproduced with permission from [47], Elsevier, 2018.

4.1. Methane-to-Methanol

Figure 4A illustrates the overall reaction mechanism for the methane-to-methanol cycle. Initially, the metal center undergoes oxidation via N_2O to create a metal oxide anionic unit (Equation (1)) [49,59]. Following this, the methane reacts with the metal oxide anion (MO^-) to generate either $HOMCH_3^-$ or $MOH^- \cdots CH_3$ (hydrogen abstraction) (Equation (2)) [100]. The former process entails the heterolytic dissociation of the CH_x and OH moieties, which then combine to form methanol, while the negative charge returns to the metal center (Equation (3)). The weaker interaction of the formed $M^- \cdots HOCH_3$ when compared to methanol with a cationic metal center enables the anionic centers to minimize the residence time of methanol at the catalytic site, thus preventing methanol overoxidation and facilitating its removal [49]. Additionally, we show later that the oxidation step poses minimal activation energy barriers for anionic centers. Given that the electron affinities of CH_4 , N_2O , and CH_3OH are small or negative (anions are unstable), and the electrons return to the metal [100].



4.2. Oxidative Coupling of Methane (OCM)

The oxidative coupling of methane (OCM) process presents an opportunity to generate ethene (C_2H_4), which holds significant value across various industrial sectors [50,101]. It serves as a vital monomer for polyethylene production and as a primary component in fuels such as gasoline (C_5 – C_{10}) or diesel (C_{10} – C_{20}) [47,50,59,68]. However, the oxidative coupling of the methane process involves a complex series of surface and gas-phase reactions that are not fully understood and can be summarized as a single global reaction, as shown in Equation (4) [47,50]. This intricate process comprises numerous oxidation and dehydration elementary reactions, yielding a range of gas-phase byproducts including H_2 , H_2O , CO_2 , CO , and C_2H_6 , alongside the desired C_2H_4 [47,50]. Minor gas-phase species like C_3H_6 , C_3H_8 , and C_2H_2 typically occur in concentrations below 1%. Although Equation (4) suggests a stoichiometric ratio of $CH_4:O_2$ as two, real-world reactors typically operate with values between five and ten to prevent the oxidation of C_2 [47].

Figure 4B outlines the schematic representation of the reaction mechanism for the oxidative coupling of methane, involving both gas-phase and surface reactions. Initially, O_2 gets adsorbed at the surface, and methane activation occurs through the formation of CH_3° radicals via surface oxygen attack. Following the formation of methyl radicals, the CH_3° radical recombination in the gas phase produces C_2H_6 , which undergoes dehydrogenation to produce C_2H_4 through attacks by H° , OH° , or CH_3° radicals, forming the ethyl radical ($C_2H_5^\circ$). Alternatively, surface oxygen attack can generate the ethyl radical ($C_2H_5^\circ$), leading to C_2H_4 production through subsequent radical attacks. Gas-phase oxygen or oxygen radical attack reactions contribute to methyl radical formation or methane activation in the gas phase and play a role in forming C_{2+} , CO_x , and H_2O species [47].



4.3. Steam Reforming of Methane

Natural gas represents a significant resource for catalytic conversions aimed at transforming methane into valuable industrial inputs and energy sources like syngas and hydrogen [27,71,84]. Figures 5–8 illustrate several important catalytic reactions for converting methane into added-value products through cleaner and more renewable processes, including the steam reforming of methane using water, the dry reforming of methane using CO_2 , electrocatalysis, and photocatalysis, which utilize electricity and sunlight as activation sources [11,26,27,71,72,76,84–86,94,101].

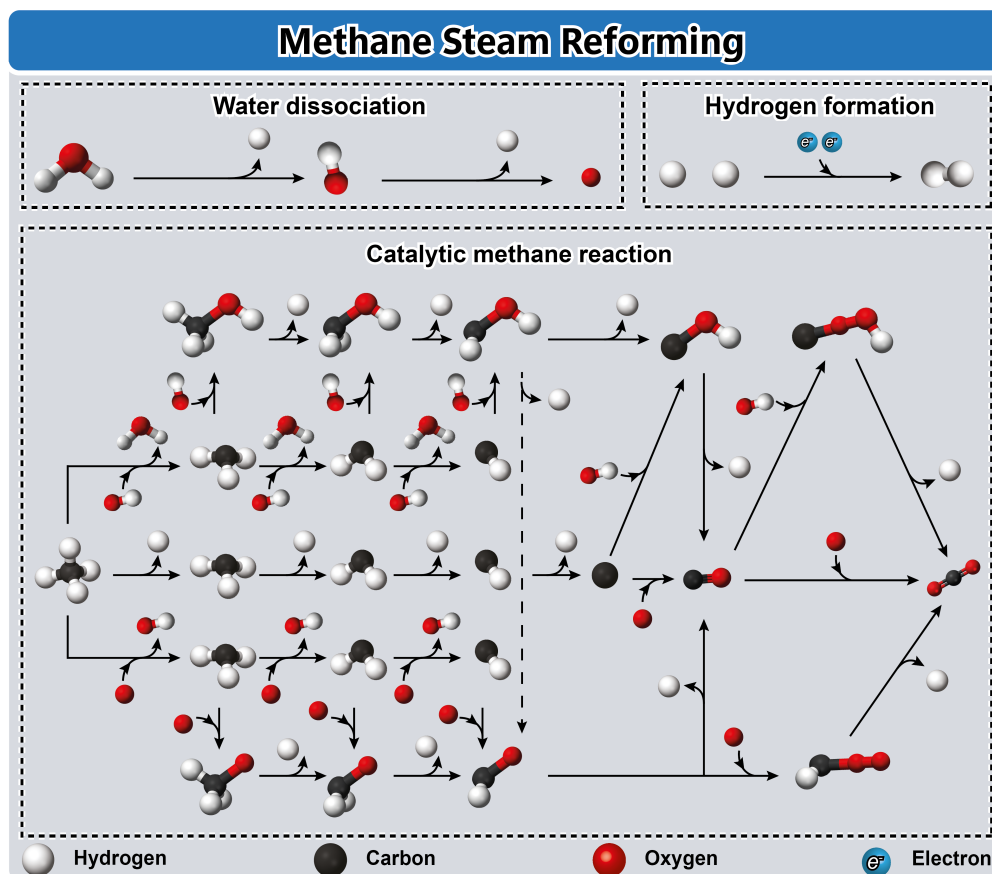


Figure 5. Schematic illustration of the catalytic reaction mechanism of steam methane reforming. Reproduced with permission from [27], Elsevier, 2022.

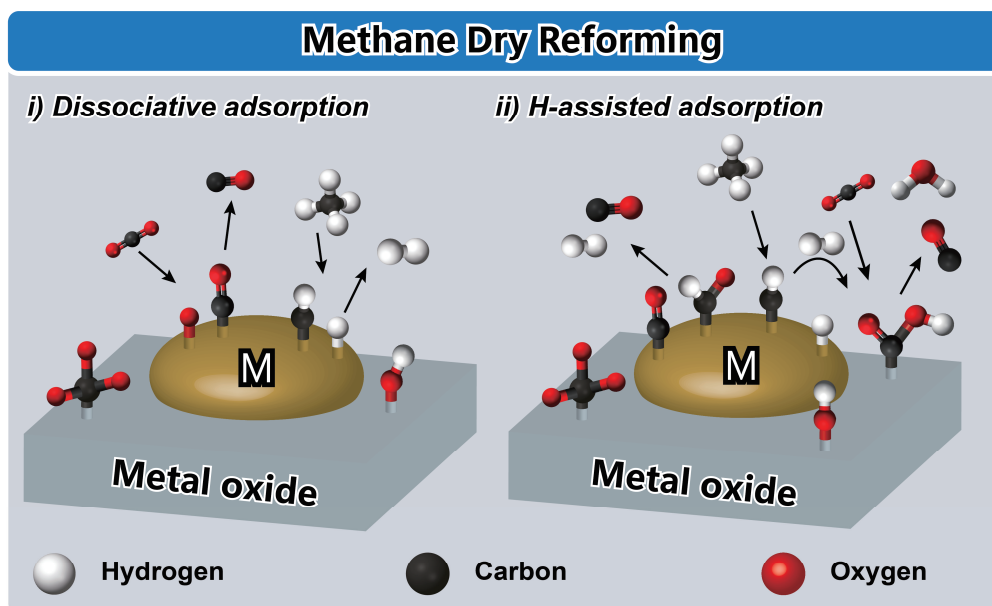


Figure 6. Schematic illustration of the catalytic reaction mechanism of the reforming of methane via (i) dissociative adsorption and (ii) H-assisted adsorption. Reproduced with permission from [102], John Wiley and Sons, 2016.

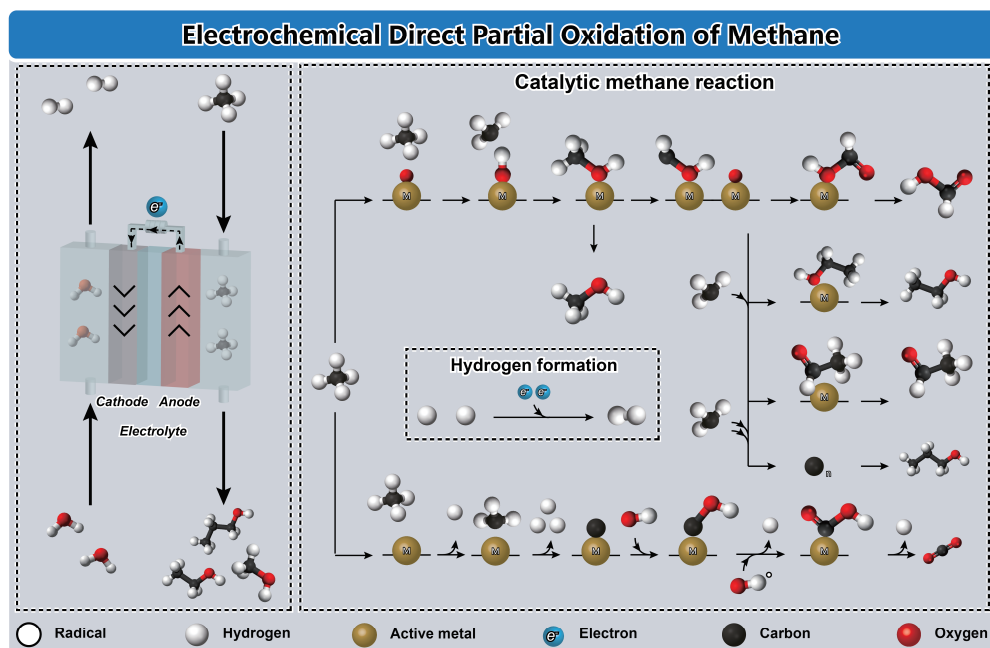


Figure 7. Schematic illustration of the catalytic reaction mechanism of the electrocatalysis of methane. Reproduced with permission from [87], John Wiley and Sons, 2020.

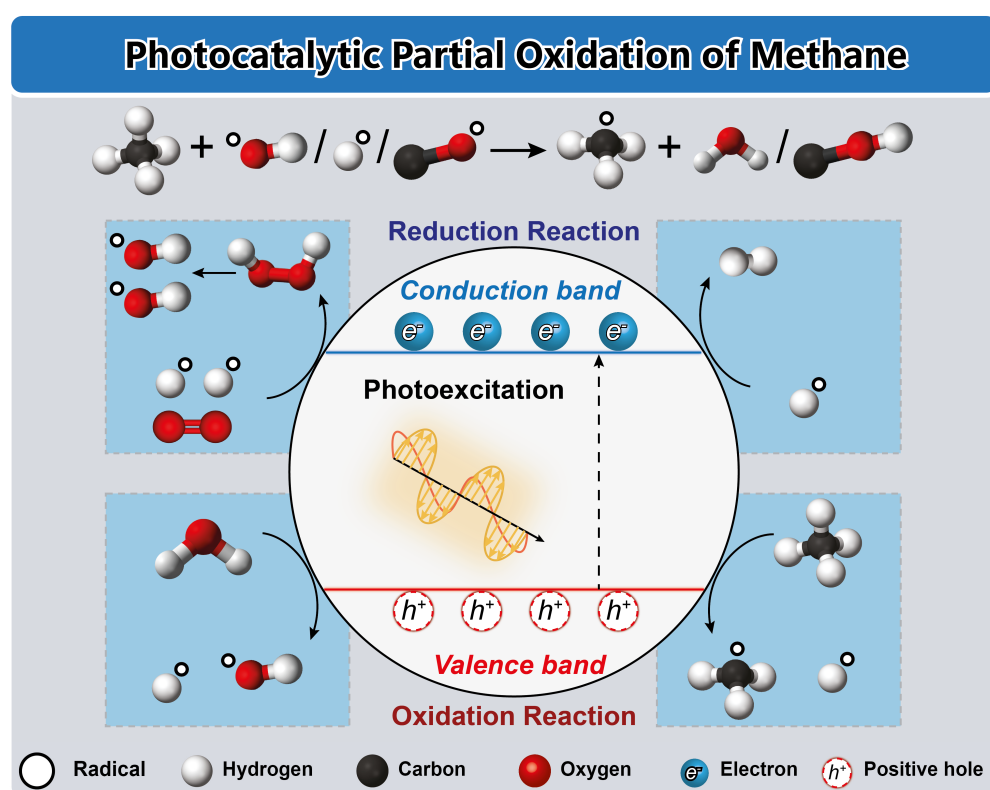


Figure 8. Schematic illustration of the catalytic reaction mechanism of the photocatalysis of methane. Reproduced with permission from [87], American Chemical Society Publications, 2023.

The steam reforming of methane for hydrogen production, depicted in Figure 5, is a pivotal process, which involves methane reacting with water vapor over a catalyst to produce hydrogen gas and carbon monoxide. Operating typically at elevated temperatures between 700 and 900 °C and moderate pressures ranging from 1 to 30 bar, the catalytic steam reforming method employs transition metal catalysts supported on high-surface-area

materials like alumina or silica [27]. Throughout the steam reforming of methane, various oxygenated species and compounds such as adsorbed surface oxygen (O), surface hydroxyl groups (OH), methoxy (CHOH), formaldehyde (CHO), and carboxyl (COOH) species play critical roles as intermediates within the reaction medium [103]. The mechanistic intricacies of steam reforming involve a series of steps [26]. Water molecules spontaneously dissociate on the catalyst surface at oxygen top sites, leading to the cleavage of O-H bonds and the formation of atomic hydrogen (H) and hydroxyl radicals (OH) [72]. These species initiate paths of C-H activation, facilitated via oxygen-assisted and hydroxyl-assisted mechanisms [104]. These activation processes involve reductive deprotonation to induce the direct dissociation of methane to CH_x (where x ranges from 0 to 3), as well as oxidation pathways yielding CH_xO and CH_xOH species [26]. Ultimately, three primary routes—redox, carboxyl, and formate mechanisms—contribute to the formation of carbon dioxide (CO_2) from carbon monoxide (CO) [72]. Finally, the combination of two hydrogen atoms culminates in the production of molecular hydrogen (H_2), representing the desired product of the steam reforming process [26,27,103].

4.4. Dry Reforming of Methane

The dry reforming of methane, as depicted in Figure 6, represents a significant pathway towards achieving sustainable development through the utilization of greenhouse gasses such as methane (CH_4) and carbon dioxide (CO_2) in chemical production, thereby mitigating environmental impact [28,77,102]. In this process, the dissociation of methane is considered the rate-determining step due to the activation of the stable C-H bond [76,105]. Upon the adsorption of methane on the metal sites, hydrogen (H_2) and CH_x species (where x represents various carbon-containing intermediates) are generated, while CO_2 undergoes dissociative adsorption on metallic particles to yield carbon monoxide (CO) and oxygen (O) [28,102]. The adsorbed oxygen species subsequently react with CH_x to form CH_xO species, which eventually dissociate to produce CO and H_2 [71,106]. The dissociation of CO_2 plays a critical role in activating methane, while oxygen species contribute to the partial oxidation of the metal particles [28,76,107].

The hydrogen generated in the initial step initiates a new bifunctional mechanism involving two types of active centers: basic sites on the support material and metallic particles [28,76]. CO_2 is adsorbed on the basic sites of the support to form carbonate/bicarbonate species, which are then transformed into CO and water (H_2O) through the formation of formate-type intermediates via H-assisted CO_2 decomposition. This latter process actively participates in the reaction mechanism through the reverse water–gas-shift reaction. The formation of formate species requires the close vicinity of carbonate species and hydrogen adsorbed on the metal surface, demonstrating the intricate interplay of multiple active sites and intermediates in the dry reforming of methane [102,106]. However, it is important to mention that, because of the metal affinity towards oxygen, the mechanism can be directed to a format near the carbonate-mediated pathway. For example, Pt, Pd, and Ag surfaces were proposed to react to a carboxyl-mediated associative mechanism, whereas Cu, Ni, and Rh metals proceed via redox mechanisms because of the stronger metal–O interaction [104,105,108,109]. Oxygen vacancy sites are important as they are able to perform the CO_2 reduction and the C=O bond cleavages over reducible supports, as Ce-Zr oxides and Fe-based catalysts are described to switch from redox to redox-associative reaction pathways via formate species [104,105,108].

4.5. Electrochemical Direct Partial Oxidation of Methane

The traditional pathways for methane conversion rely on thermal activation, necessitating harsh reaction conditions such as high temperatures (>700 °C) and pressures (>2.5 bar) to initiate C-H bond dissociation [84,87]. However, alternative methods such as electrochemical and photo-based methane conversion technologies offer activation through electricity and light [84]. Electrochemical-based conversions allow precise control over product formation via the utilization of surface energy through electrode potential [85,88].

Figure 7 illustrates the electrochemical direct partial oxidation of methane, which faces challenges in directly activating methane using electrocatalysts and adjusting the pH of the aqueous electrolyte [87]. In low pH solutions, methane can be activated over metal catalysts using the potentiodynamic concept via applying potential on a given catalyst for an extended period [85]. Conversely, most electrocatalysts enhance methane activation under high pH conditions, where they interact with oxidants like O_2 , CO_3^{2-} , and OH^- to activate the CH_4 molecule. Mechanistically, the catalyst should weakly bind oxygen or bind it as a radical at a suitable potential for oxidizing methane while preventing oxygen evolution [87,110]. Thus, selectivity towards desired products relies on factors such as the availability of adsorbed oxygen ion species, high oxygen vacancy on the catalyst, and the extent of exposed oxide species [84,86]. The activation of the methane molecule involves abstracting H or introducing O, leading to the formation of C_1 species on the catalyst surface. Metal electrocatalysts promote total methane oxidation into CO_2 , while oxo-included catalysts facilitate partial oxidation into various oxygenates like CH_3OH , $HCHO$, CO , and $HCOO^-$ [85,86,110]. Formaldehyde forms as a methanol oxidation product, then undergoes attachment by a methyl free radical to form an acetaldehyde intermediate, which can further oxidize into C_3 alcohols and ketones through electrophilic attachment [87,110]. The *CH_2 intermediate is hydroxylated thermodynamically before coupling with a methyl radical to produce the final ethanol product [84]. Finally, the combination of two hydrogen atoms culminates in the production of molecular hydrogen (H_2) [84,85].

4.6. Photocatalytic Direct Partial Oxidation of Methane

Photocatalytic methane conversion represents a promising avenue for transforming methane into valuable chemical products under mild conditions, harnessing solar energy as a sustainable and environmentally friendly activation source [9]. Photocatalysts absorb photons, generating energetic carriers (electrons and holes) that can activate and convert methane molecules. This disruption of the thermodynamic equilibrium enables uphill reactions to occur at room temperature, helping to mitigate catalyst deactivation to some extent [9,11,67,77,93–95,111].

Upon light radiation, the photoexcitation of electrons (e^-) from the valence band to the conduction band creates positive holes (h^+) in the valence band [94]. The energy levels at the bottom of the conduction band and the top of the valence band determine the reducing and oxidizing abilities of photoelectrons and photogenerated holes, respectively [11]. Electrons can react with molecular oxygen to produce peroxide and radical oxygen, leading to the degradation of organic compounds into CO_2 and H_2O , or they can directly interact with organic compounds to yield reduction products [9]. Meanwhile, holes can react with water to produce hydroxyl radicals, which subsequently oxidize organic compounds or directly interact with them [112]. In methane conversion, an ideal catalyst should achieve the partial oxidation of methane to high-value products, thereby enhancing the utilization value of methane [11]. To improve selectivity towards high-value products, appropriate active sites must be introduced to regulate the formation of free radicals, activation barriers of intermediates, and adsorption/desorption of intermediates [94]. Methane can be converted into various products, including gaseous (C_2H_6 , C_2H_4 , and C_3H_8) and liquid (CH_3OOH , CH_3OH , CH_3CH_2OH , $HCHO$, and $HCOOH$) products, with the type of products depending on the reaction systems employed [11].

In Figure 8, the activation of the C-H bond in methane conversion through photocatalysis follows two main pathways: direct and indirect. The valence band of metal oxides, primarily composed of O 2p orbitals, possesses positive potential and strong oxidation ability for CH_4 activation. Upon light irradiation, the surface lattice oxygen of metal oxides can trap photogenerated holes (h^+), leading to the generation of reactive oxygen species ($O=$), which can directly capture the H atom from CH_4 , generating $\bullet CH_3$ radicals. In the indirect route, C-H bond cleavage can be initiated by oxygen radicals such as $\bullet OH$, generated through the reaction between photogenerated carriers and adsorbate [9,11,94,95,112].

Interestingly, it is noted that in all examples of methane conversion reactions, nanomaterials can be optimized for specific surface properties such as controlled surface defects like oxygen vacancies, reducibility, acidity, basicity, electronic activity, and surface properties tailored to a particular reaction [12,37,38,42,44,45].

5. Comparative Analysis with Traditional Catalysts

In the earlier sections, we explored various techniques involving the interaction of methane with catalyst surfaces, underscoring the vital role played by nanomaterials in enhancing methane conversion. When materials are scaled down from the macroscopic level to the nanoscale (ranging from 1 up to ~100 nm), significant changes occur in their surface-to-volume ratio, lattice parameters, and surface energy. This reduction in lattice parameters modifies the geometric and electronic structures of the material by adjusting the distances between atoms in the crystalline lattice, resulting in improved properties when compared to larger-scale counterparts. Additionally, not only the size but also the shape of nanomaterials strongly affects properties such as surface reactivity, electrochemical behavior, optical characteristics, and photocatalytic performance.

Premachandra Heagy conducted a study examining how the size and shape of WO_3 micro- and nanomaterials influence photocatalytic properties, particularly in the conversion of methane to methanol. This investigation compared materials with uncontrolled morphologies, such as microparticles and nanoparticles, with precisely engineered structures including nanorods, nanowires, and nanoflowers. The scanning electron microscopy (SEM) images depicted in Figure 9 illustrate the diverse morphologies and sizes of WO_3 materials, alongside spectroscopic data, and the efficiency of methane-to-methanol conversion. While uncontrolled materials display irregular shapes and sizes, the engineered structures like nanorods, nanowires, and nanoflowers exhibit uniform morphology. However, nanorods are prone to particle aggregation. The analysis of the specific surface area indicates that controlled morphologies have higher surface areas, thereby improving optical and electronic properties.

Figure 9G,H present UV-vis and photoluminescence emission spectra of WO_3 materials. Nanoflowers exhibit the highest rates of photocatalysis and selectivity towards methanol production, attributed to the slower recombination of photogenerated carriers on the surface and a larger specific surface area, allowing for the increased generation of surface-bound hydroxyl radicals. The 3D hierarchical structure of nanoflowers, characterized by petal-like nanosheet structures and hollow chambers, facilitates multiple reflections of light, resulting in the enhanced formation of photogenerated electron/hole pairs due to improved light interaction with the material surface. In contrast, nanorods and nanowires show similar levels of methanol production, surface areas, and band gap energy.

As another example of support shape effects, La_2O_3 catalysts with various morphologies such as nanoparticles, flower-like structures, nanorods, nanofibers, and nanospheres were employed for the oxidative coupling of methane [111]. The different morphologies exhibited distinct physicochemical properties; for instance, La_2O_3 nanospheres displayed moderately strong acidic sites, whereas La_2O_3 nanorods and nanofibers exhibited weak acidic sites, and nanoparticles and flower-like structures did not display any acidic sites. In terms of basic sites, all morphologies showed weak and moderate basic sites with significant differences between them, with values of 4.9, 3.5, 31.9, 13.9, and 5.8 $\mu\text{mol}\cdot\text{g}^{-1}$ of total surface basicity. Moreover, the morphological differences also affected the catalytic properties of the La_2O_3 catalysts. Nanoparticles, flower-like structures, and nanospheres exhibited methane conversion and C_2 selectivity above 480 or 510 °C, whereas nanorods and nanofibers exhibited methane conversion and C_2 selectivity at 450 °C. Interestingly, nanofibers and nanoparticles displayed the highest C_2 selectivity (45%), while flower-like structures, nanorods, and nanospheres exhibited 35% C_2 selectivity. Additionally, the temperature at which the reaction initiated increased with the binding energy of lattice oxygen [111]. An increase in the binding energy of lattice oxygen suggests a shift in its nature from nucleophilic to electrophilic [113,114]. Consequently, a more nucleophilic O^{2-}

and a more electrophilic La^{3+} pair could lower the activation energy required for C-H bond cleavage, initiating the reaction at lower temperatures. Moreover, there was an observed trend indicating that the initiation temperature of the reaction decreased with increasing surface basicity. This suggests that an abundance of nucleophilic surface sites promotes low methane activation since CO_2 acts as an electron acceptor and reflects electron density on the surface [111].

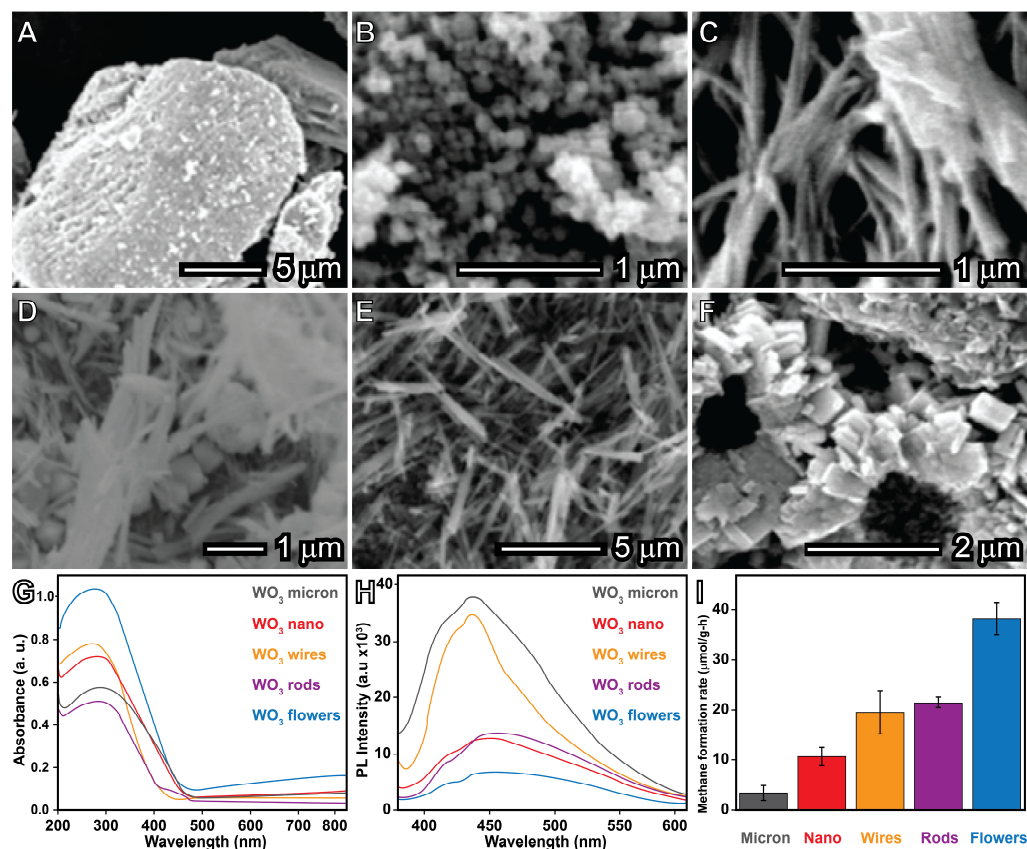


Figure 9. Comparison between bulk and nanocatalysts. Scanning electron microscopy (SEM) images of WO₃ micron particles (A), WO₃ nanoparticles (B), WO₃ nanowires (C,D), WO₃ nanorods (E), WO₃ nanoflowers (F), optical properties via UV-vis spectra (G) and photoluminescence spectroscopy (H), and methane conversion ratio (I) [115].

For instance, in methane oxidation, Ni/CeO₂ nanoparticles, nanorods, and nanocubes were utilized in methane oxidation [116]. The different morphologies exhibited distinct properties; for example, CeO₂ nanocubes expose the (100) surface facet, which has lower surface free energy, a lower specific surface area, and lower oxygen storage capacity [12,117]. CeO₂ nanoparticles displayed the lowest oxygen storage capacity and specific surface area due to their well-crystallized nature, with a crystallite size of 45.6 nm. Conversely, CeO₂ nanorods showed a higher oxygen storage capacity, with the (111) surface facet exposed, having higher surface free energy and a higher specific surface area. These morphological differences in the properties of the nanostructures are reflected in their catalytic activity towards methane oxidation, which increases with the amount of surface oxygen vacancies and oxygen storage capacity, in the order of nanorods > nanoparticles > nanocubes [116].

In a well-controlled synthesis example, Ga₂O₃ microrods were combined with Pt nanoparticles with particle sizes ranging from 1.5 to 2.7 nm for the photocatalytic coupling of methane. The Ga₂O₃ microrods were synthesized via a template-free solvothermal method using ethanol/water as the solvent. This process resulted in the formation of microprisms of CaOOH, which were then annealed to produce mesoporous microrods, which measured 4–5 μm in length and 200–300 nm in width (Figure 10A,B). Pt nanoparticles

were subsequently photodeposited onto the surface of the Ga₂O₃ microrods to achieve well-controlled sizes of 1.5, 1.9, 2.2, 2.5, and 2.7 nm, resulting in highly dispersed Pt nanoparticle distribution (Figure 10C,D). The particle size of the Pt nanoparticles extended the absorption range into the visible-light region and increased the band gap of the composite material [118].

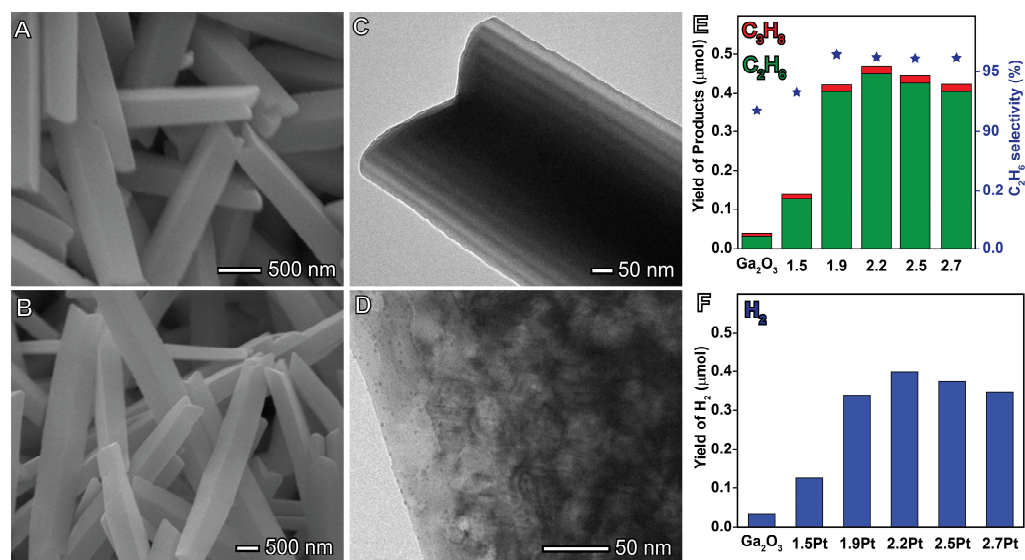


Figure 10. Case study of controlled nanocatalysts Pt/Gd₂O₃ to photocatalytic reactions. Scanning electron microscopy (SEM) and transmission scanning electron (TEM) images of Gd₂O₃ (A,C) and Pt/Gd₂O₃ (B,D), yield and selective of coupling products, which are ethane and propane, shown in green and red, respectively for yield, and the stars for ethane selectivity (E), and hydrogen yield (F). Reproduced with permission from [87], American Chemical Society Publications, 2021.

Jiayu Ma et al. observed that the interaction between Pt nanoparticles and Ga₂O₃ microrods led to the partial oxidation of Pt^{δ+} (Pt²⁺ and Pt⁴⁺) through an electron transfer from Ga₂O₃ to Pt, consequently increasing the number of oxygen vacancies. These enhanced properties effectively facilitated the conversion of methane to ethane (as shown in Equation (5)). The size effect of Pt on the nonoxidative coupling of methane photocatalytic activity was investigated, revealing that the corner Pt atoms served as geometrically active sites for CH₄ activation, while Pt^{δ+} species distributed on the terrace sites assisted in C-H polarization. Additionally, PtO₂ promoted the transfer of a photoinduced hole from Ga₂O₃ to oxidize adsorbed -CH₃ in order to form a •CH₃ radical. Figure 10E,F illustrate the selectivity and yield to ethane, hydrogen, and propane. Ga₂O₃ microrods exhibited lower values, while the incorporation of Pt nanoparticles strongly influenced the photocatalytic activity, leading to improved performance [118].



In another well-controlled synthesis example, titanate nanotubes were combined with gold nanoparticles ranging in size from 1 to 9 nm for the photocatalytic coupling of methane [119]. Titanate nanotubes, characterized by open-ended hollow cylinders measuring up to 200 nm in length and 15 nm in outer diameter, are of great interest for catalytic applications due to their high surface area and cation exchange capacity, which facilitate achieving high metal dispersion. Ion exchange allows titanate nanotubes to incorporate metal adatoms into their framework, and the curved layers contain a large number of defect sites, typically oxygen vacancies and Ti³⁺ centers, which can make them promising photocatalysts because the defect sites can trap photoelectrons or holes, thus extending the lifetime of the excited state. Gold nanoparticles smaller than 3 nm lose their

bulk-like electronic properties; for example, they no longer exhibit the plasmon excitation characteristics of relatively large gold nanocrystals [119–123].

Kiss et al. observed that smaller gold nanoparticles exhibit methane conversion, hydrogen, and ethane formation which are four times higher than larger gold nanoparticles, at 1.6% and 0.4%, 116 and 48 $\mu\text{mol}\cdot\text{h}^{-1}\cdot\text{g}^{-1}$ of H_2 , and 12.0 and 1.5 $\mu\text{mol}\cdot\text{h}^{-1}\cdot\text{g}^{-1}$ of C_2H_6 , respectively. In agreement, László et al. observed that gold nanoparticles supported in titanate nanotubes produced eight times more C_2H_6 and three times more H_2 [122]. This remarkable catalytic activity can be explained by the fact that electron–hole pairs are generated on gold-promoted titanate nanotubes upon the absorption of UV light [124]. After the dissociation of the exciton, the electron and the hole migrate to energetically favorable positions. Electrons have a higher possibility of being found on the metal particles due to the Fermi-level equilibration between the metal and the oxide [125]. Surface water molecules can catch the hole and produce reactive OH radicals and H^+ that delocalize onto nearby water molecules. The as-generated hydroxyl radicals are very aggressive oxidants and start to oxidize methane in a radical-type reaction. The formed methyl radical adsorbs onto the metal surface. The methyl radical decomposes consecutively into hydrogen and carbon or recombines to form ethane [119]. In small dimensions, the plasmonic feature does not operate. However, multiple molecular-like transitions of the gold cluster with a partial positive charge can bind strongly to the defect sites in titanate nanotubes. These clusters may be directly involved in the photo-induced reactions, namely in the direct activation of the methane/ $\text{Au}_{25}^{\delta+}$ complex during irradiation (Equation (6)).



As an example for the dry reforming of methane, NiCo nanoparticles supported by ZrO_2 hollow nanospheres were applied in the dry reforming of methane reaction [126]. In this case, rational catalyst synthesis can lead to the production of nanomaterials with higher catalytic activity and long-term stability. Ni and Co act as catalysts for methane cracking and CO_2 reduction, respectively, and the induced carbon deposition and active oxygen combine to release CO in order to regenerate the metal surface. Moreover, the hollow ZrO_2 nanospheres exhibited higher activity and better stability due to strong metal–support interactions and the effective mass transportation of the reactants and products [126].

As an example for the methane-to-methanol reaction, Pd@Pt core–shell nanoparticles were evaluated in the methane-to-methanol reaction [127]. The combination of Pd in the core and Pt in the shell promotes enhanced electronic properties of the catalyst. Pd donates electrons to Pt, leading to a higher surface electron density, higher rates of methane activation, and high selectivity and productivity towards methanol. In comparison, monometallic Pt nanoparticles exhibited high selectivity to methanol but low methane conversion, while monometallic Pd nanoparticles showed high selectivity to formaldehyde. In bimetallic alloy PdPt nanoparticles, a range of compositions from 1:1 to 8:1 or 1:8 was reported. However, when the ratio of Pt:Pd shifted from 1:1 to 1:8, there was a decrease in methanol selectivity, likely due to the exposed Pd. Additionally, Pt@Pd core–shell nanoparticles, with Pt in the core and Pd in the shell, exhibited lower primary oxygenate selectivity [127].

For instance, in the context of methane steam reforming, a study investigated the impact of size and metal variation ($M = \text{Ni}, \text{Pd}, \text{Pt}, \text{and Rh}$) on catalytic performance. This investigation utilized computational density functional theory (DFT) and microkinetic modeling [128]. The truncated octahedron structure was used to simulate a spherical nanoparticle in TEM images, enabling the exploration of the influence of three primary exposed particle surfaces ($M(111)$, $M(211)$, and $M(100)$) on catalytic behavior [129–131]. Furthermore, the study revealed how nanoparticle size alters the ratio between these exposed surfaces and their respective significance in catalytic properties. The activity dependency on nanoparticle size was found to be closely linked to surface characteristics [132,133]. At smaller particle sizes, the dominance of the $M(211)$ surface exposure was noted, whereas larger particles saw increasing contributions from $M(111)$ and $M(100)$. However, the en-

ergetics favored M(211) over M(111), and the activity of M(100) was limited by surface site blockage. Consequently, larger particles exhibited reduced activity due to the lower activity of M(100) and M(111) surfaces when compared to M(211) [129–133]. In terms of metal-dependent activity, the study found that Rh exhibited the highest activity, followed by Ni, and then Pd and Pt, which showed similar levels of activity. This difference in activity was attributed to the high free energy barriers observed for Pd and Pt, while Ni activity was constrained by surface blockage.

6. Conclusions: Challenges and Future Perspectives

Significant advances have been made in controlled nanocatalysts for methane reactions, with a focus on understanding and manipulating synthetic parameters to control surface and nanomaterial properties. This review emphasizes exploring the differences between bulk and nanomaterial properties regarding reaction selectivity. The discussion begins with an examination of catalyst property engineering at the nanoscale, which has unlocked unprecedented control over reaction pathways, selectivity, and stability. By leveraging advanced synthesis techniques and insightful characterization methods, surface functionalities, catalytic sites, and synthetic parameters underscore the pivotal role of nanotechnology in tailoring catalysts for methane conversion. Whether through homolytic radical mechanisms or heterolytic surface-stabilized pathways, designing nanomaterials with engineered surfaces and optimized electronic structures has unlocked new avenues for enhancing methane activation efficiency and selectivity. Harnessing the unique properties of nanoscale materials, such as surface defects, morphology, and composition, the exploration of the reaction mechanisms and kinetics of methane in sustainable energy production highlights the intricate interplay between catalysts, reaction conditions, and product selectivity. Through the utilization of controlled nanocatalysts and optimizing methane conversion pathways, ranging from methane-to-methanol cycles to oxidative coupling, these pathways offer promising routes for transforming methane into valuable products such as methanol, ethene, and hydrogen, with applications spanning various industrial sectors. Moreover, emerging technologies such as electrochemical and photocatalytic methane conversion present exciting opportunities for achieving cleaner and more renewable processes, harnessing electricity and sunlight as activation sources. The ability to tailor nanomaterial properties, including surface defects, reducibility, and electronic properties, underscores the critical role of nanotechnology in advancing sustainable energy production. Lastly, the comparative analysis with traditional catalysts underscores the transformative impact of nanomaterials on methane conversion processes. Through meticulous control over the size, shape, and composition, nanocatalysts exhibit superior performance when compared to their macroscopic counterparts. Studies investigating the photocatalytic properties of materials like WO_3 , Ga_2O_3 microrods, and titanate nanotubes coupled with Pt or Au nanoparticles reveal enhanced methane-to-methanol and methane-to-ethane conversion rates, and have also explored other examples of catalytic reactions, highlighting the pivotal role of nanotechnology in advancing catalytic efficiency and emphasizing the importance of nanoscale engineering in achieving remarkable catalytic activity. In this context, this review posits that advancements in nanocatalyst synthesis, enabling the precise comparison of bulk and nanomaterials on methane conversion, are pivotal for enhancing our comprehension of catalysis, driving progress in the fields of methane, chemistry, and nanoscience.

Author Contributions: Writing—original draft preparation, F.A.e.S.; writing—review and editing, T.S.R. All authors have read and agreed to the published version of the manuscript.

Funding: We are grateful to the Fundação de Amparo à Pesquisa do Estado do Rio de Janeiro (FAPERJ), grant numbers E-26/201.431/2021 and E-26/211.612/2019; to the Conselho Nacional de Desenvolvimento Científico e Tecnológico—CNPq, grant number 317288/2021-0; and to the Coordenação de Aperfeiçoamento de Pessoal de Nível Superior—Brasil (CAPES)—Finance Code 001, grant number 88887.645934/2021-00.

Institutional Review Board Statement: Not applicable.

Informed Consent Statement: Not applicable.

Data Availability Statement: Not applicable.

Conflicts of Interest: The authors declare no conflicts of interest.

References

1. Chen, R.; Weng, G. Sustainable Energy Resources for Driving Methane Conversion. *Adv. Energy Mater.* **2023**, *13*, 2301734. [[CrossRef](#)]
2. Hameed, S.; Comini, E. Methane Conversion for Hydrogen Production: Technologies for a Sustainable Future. *Sustain. Energy Fuels* **2024**, *8*, 670–683. [[CrossRef](#)]
3. Trovarelli, A.; Llorca, J. Ceria Catalysts at Nanoscale: How Do Crystal Shapes Shape Catalysis? *ACS Catal.* **2017**, *7*, 4716–4735. [[CrossRef](#)]
4. Gao, X.; Wen, Y.; Tan, R.; Huang, H.; Kawi, S. A Review of Catalyst Modifications for a Highly Active and Stable Hydrogen Production from Methane. *Int. J. Hydrogen Energy* **2023**, *48*, 6204–6232. [[CrossRef](#)]
5. Latimer, A.A.; Aljama, H.; Kakekhani, A.; Yoo, J.S.; Kulkarni, A.; Tsai, C.; Garcia-Melchor, M.; Abild-Pedersen, F.; Nørskov, J.K. Mechanistic Insights into Heterogeneous Methane Activation. *Phys. Chem. Chem. Phys.* **2017**, *19*, 3575–3581. [[CrossRef](#)] [[PubMed](#)]
6. Kopp Alves, A.; Bergmann, C.P.; Berutti, F.A. *Novel Synthesis and Characterization of Nanostructured Materials*; Springer: Berlin/Heidelberg, Germany, 2013; ISBN 978-3-642-41274-5.
7. Chen, J.; Zhang, Y.; Zhang, Z.; Hou, D.; Bai, F.; Han, Y.; Zhang, C.; Zhang, Y.; Hu, J. Metal–Support Interactions for Heterogeneous Catalysis: Mechanisms, Characterization Techniques and Applications. *J. Mater. Chem. A Mater.* **2023**, *11*, 8540–8572. [[CrossRef](#)]
8. Li, Y.; Zhang, Y.; Qian, K.; Huang, W. Metal–Support Interactions in Metal/Oxide Catalysts and Oxide–Metal Interactions in Oxide/Metal Inverse Catalysts. *ACS Catal.* **2022**, *12*, 1268–1287. [[CrossRef](#)]
9. Li, X.; Wang, C.; Tang, J. Methane Transformation by Photocatalysis. *Nat. Rev. Mater.* **2022**, *7*, 617–632. [[CrossRef](#)]
10. Li, C.; Clament Sagaya Selvam, N.; Fang, J. Shape-Controlled Synthesis of Platinum-Based Nanocrystals and Their Electrocatalytic Applications in Fuel Cells. *Nanomicro Lett.* **2023**, *15*, 83. [[CrossRef](#)]
11. Liu, Z.; Xu, B.; Jiang, Y.-J.; Zhou, Y.; Sun, X.; Wang, Y.; Zhu, W. Photocatalytic Conversion of Methane: Current State of the Art, Challenges, and Future Perspectives. *ACS Environ. Au* **2023**, *3*, 252–276. [[CrossRef](#)]
12. Rodrigues, T.S.; de Moura, A.B.L.; e Silva, F.A.; Candido, E.G.; da Silva, A.G.M.; de Oliveira, D.C.; Quiroz, J.; Camargo, P.H.C.; Bergamaschi, V.S.; Ferreira, J.C.; et al. Ni Supported Ce_{0.9}Sm_{0.1}O_{2-δ} Nanowires: An Efficient Catalyst for Ethanol Steam Reforming for Hydrogen Production. *Fuel* **2019**, *237*, 1244–1253. [[CrossRef](#)]
13. Rodrigues, T.S.; da Silva, A.G.M.; Camargo, P.H.C. Nanocatalysis by Noble Metal Nanoparticles: Controlled Synthesis for the Optimization and Understanding of Activities. *J. Mater. Chem. A Mater.* **2019**, *7*, 5857–5874. [[CrossRef](#)]
14. Huo, D.; Kim, M.J.; Lyu, Z.; Shi, Y.; Wiley, B.J.; Xia, Y. One-Dimensional Metal Nanostructures: From Colloidal Syntheses to Applications. *Chem. Rev.* **2019**, *119*, 8972–9073. [[CrossRef](#)] [[PubMed](#)]
15. Qamar, O.A.; Jamil, F.; Hussain, M.; Bae, S.; Inayat, A.; Shah, N.S.; Waris, A.; Akhter, P.; Kwon, E.E.; Park, Y.-K. Advances in Synthesis of TiO₂ Nanoparticles and Their Application to Biodiesel Production: A Review. *Chem. Eng. J.* **2023**, *460*, 141734. [[CrossRef](#)]
16. e Silva, F.; Salim, V.; Rodrigues, T. Controlled Nickel Nanoparticles: A Review on How Parameters of Synthesis Can Modulate Their Features and Properties. *AppliedChem* **2024**, *4*, 86–106. [[CrossRef](#)]
17. Harish, V.; Ansari, M.M.; Tewari, D.; Yadav, A.B.; Sharma, N.; Bawarig, S.; García-Betancourt, M.-L.; Karatutlu, A.; Bechelany, M.; Barhoum, A. Cutting-Edge Advances in Tailoring Size, Shape, and Functionality of Nanoparticles and Nanostructures: A Review. *J. Taiwan. Inst. Chem. Eng.* **2023**, *149*, 105010. [[CrossRef](#)]
18. França, M.C.; Ferreira, R.M.; dos Santos Pereira, F.; Silva, F.A.; Silva, A.C.A.; Cunha, L.C.S.; Varela Júnior, J.d.J.G.; de Lima Neto, P.; Takana, A.A.; Rodrigues, T.S.; et al. Galvanic Replacement Managing Direct Methanol Fuel Cells: AgPt Nanotubes as a Strategy for Methanol Crossover Effect Tolerance. *J. Mater. Sci.* **2022**, *57*, 8225–8240. [[CrossRef](#)]
19. Xie, C.; Niu, Z.; Kim, D.; Li, M.; Yang, P. Surface and Interface Control in Nanoparticle Catalysis. *Chem. Rev.* **2020**, *120*, 1184–1249. [[CrossRef](#)] [[PubMed](#)]
20. da Silva, M.V.; Fajardo, H.V.; Rodrigues, T.S.; e Silva, F.A.; Bergamaschi, V.S.; Dias, A.; Siqueira, K.P.F. Synthesis of NiMoO₄ Ceramics by Proteic Sol-Gel Method and Investigation of Their Catalytic Properties in Hydrogen Production. *Mater. Chem. Phys.* **2021**, *262*, 124301. [[CrossRef](#)]
21. Li, Z.; Xiao, Y.; Chowdhury, P.R.; Wu, Z.; Ma, T.; Chen, J.Z.; Wan, G.; Kim, T.-H.; Jing, D.; He, P.; et al. Direct Methane Activation by Atomically Thin Platinum Nanolayers on Two-Dimensional Metal Carbides. *Nat. Catal.* **2021**, *4*, 882–891. [[CrossRef](#)]
22. Rangel de Melo Rodrigues, M.; Machado Ferreira, R.; dos Santos Pereira, F.; Anchieta e Silva, F.; César Azevedo Silva, A.; Aguilar Vitorino, H.; de Jesus Gomes Varela Júnior, J.; Atsushi Tanaka, A.; Aurélio Suller Garcia, M.; Silva Rodrigues, T. Application of AgPt Nanoshells in Direct Methanol Fuel Cells: Experimental and Theoretical Insights of Design Electrocatalysts over Methanol Crossover Effect. *ChemCatChem* **2022**, *14*, 2200605. [[CrossRef](#)]

23. Vieira, L.H.; Rasteiro, L.F.; Santana, C.S.; Catuzo, G.L.; da Silva, A.H.M.; Assaf, J.M.; Assaf, E.M. Noble Metals in Recent Developments of Heterogeneous Catalysts for CO₂ Conversion Processes. *ChemCatChem* **2023**, *15*, 2300493. [[CrossRef](#)]
24. Al-Fatesh, A.S.; Patel, N.; Fakeeha, A.H.; Alotibi, M.F.; Alreshaidan, S.B.; Kumar, R. Reforming of Methane: Effects of Active Metals, Supports, and Promoters. *Catal. Rev.* **2023**, *5*, 1–99. [[CrossRef](#)]
25. Taherian, Z.; Khataee, A.; Han, N.; Orooji, Y. Hydrogen Production through Methane Reforming Processes Using Promoted-Ni/Mesoporous Silica: A Review. *J. Ind. Eng. Chem.* **2022**, *107*, 20–30. [[CrossRef](#)]
26. Niu, J.; Wang, Y.; Qi, Y.; Dam, A.H.; Wang, H.; Zhu, Y.-A.; Holmen, A.; Ran, J.; Chen, D. New Mechanism Insights into Methane Steam Reforming on Pt/Ni from DFT and Experimental Kinetic Study. *Fuel* **2020**, *266*, 117143. [[CrossRef](#)]
27. Wang, F.; Li, Y.; Wang, Y.; Zhang, C.; Chu, L.; Yang, L.; Fan, X. Mechanism Insights into Sorption Enhanced Methane Steam Reforming Using Ni-Doped CaO for H₂ Production by DFT Study. *Fuel* **2022**, *319*, 123849. [[CrossRef](#)]
28. Wittich, K.; Krämer, M.; Bottke, N.; Schunk, S.A. Catalytic Dry Reforming of Methane: Insights from Model Systems. *ChemCatChem* **2020**, *12*, 2130–2147. [[CrossRef](#)]
29. Kumar, G.; Lau, S.L.J.; Krcha, M.D.; Janik, M.J. Correlation of Methane Activation and Oxide Catalyst Reducibility and Its Implications for Oxidative Coupling. *ACS Catal.* **2016**, *6*, 1812–1821. [[CrossRef](#)]
30. Li, Z.; Chen, Y.; Xie, Z.; Song, W.; Liu, B.; Zhao, Z. Rational Design of the Catalysts for the Direct Conversion of Methane to Methanol Based on a Descriptor Approach. *Catalysts* **2023**, *13*, 1226. [[CrossRef](#)]
31. Fujimoto, Y.; Ohba, T. Size-Dependent Catalytic Hydrogen Production via Methane Decomposition and Aromatization at a Low-Temperature Using Co, Ni, Cu, Mo, and Ru Nanometals. *Phys. Chem. Chem. Phys.* **2022**, *24*, 28794–28803. [[CrossRef](#)]
32. Sharifianjazi, F.; Esmailkhanian, A.; Bazli, L.; Eskandarinezhad, S.; Khaksar, S.; Shafiee, P.; Yusuf, M.; Abdullah, B.; Salahshour, P.; Sadeghi, F. A Review on Recent Advances in Dry Reforming of Methane over Ni- and Co-Based Nanocatalysts. *Int. J. Hydrogen Energy* **2022**, *47*, 42213–42233. [[CrossRef](#)]
33. Gangarajula, Y.; Hong, F.; Li, Q.; Jiang, X.; Liu, W.; Akri, M.; Su, Y.; Zhang, Y.; Li, L.; Qiao, B. Operando Induced Strong Metal-Support Interaction of Rh/CeO₂ Catalyst in Dry Reforming of Methane. *Appl. Catal. B* **2024**, *343*, 123503. [[CrossRef](#)]
34. Szécsényi, Á.; Li, G.; Gascon, J.; Pidko, E.A. Unraveling Reaction Networks behind the Catalytic Oxidation of Methane with H₂O₂ over a Mixed-Metal MIL-53(Al,Fe) MOF Catalyst. *Chem. Sci.* **2018**, *9*, 6765–6773. [[CrossRef](#)] [[PubMed](#)]
35. Hofman, M.S.; Wang, D.Z.; Yang, Y.; Koel, B.E. Interactions of Incident H Atoms with Metal Surfaces. *Surf. Sci. Rep.* **2018**, *73*, 153–189. [[CrossRef](#)]
36. Latimer, A.A.; Kulkarni, A.R.; Aljama, H.; Montoya, J.H.; Yoo, J.S.; Tsai, C.; Abild-Pedersen, F.; Studt, F.; Nørskov, J.K. Understanding Trends in C-H Bond Activation in Heterogeneous Catalysis. *Nat. Mater.* **2017**, *16*, 225–229. [[CrossRef](#)]
37. Su, J.; Zou, X.; Chen, J.-S. Self-Modification of Titanium Dioxide Materials by Ti³⁺ and/or Oxygen Vacancies: New Insights into Defect Chemistry of Metal Oxides. *RSC Adv.* **2014**, *4*, 13979–13988. [[CrossRef](#)]
38. Dhall, A.; Self, W. Cerium Oxide Nanoparticles: A Brief Review of Their Synthesis Methods and Biomedical Applications. *Antioxidants* **2018**, *7*, 97. [[CrossRef](#)] [[PubMed](#)]
39. Tsunekawa, S.; Wang, J.-T.; Kawazoe, Y. Lattice Constants and Electron Gap Energies of Nano- and Subnano-Sized Cerium Oxides from the Experiments and First-Principles Calculations. *J. Alloys Compd.* **2006**, *408–412*, 1145–1148. [[CrossRef](#)]
40. Zhou, X.-D.; Huebner, W. Size-Induced Lattice Relaxation in CeO₂ Nanoparticles. *Appl. Phys. Lett.* **2001**, *79*, 3512–3514. [[CrossRef](#)]
41. Tsunekawa, S.; Sahara, R.; Kawazoe, Y.; Ishikawa, K. Lattice Relaxation of Monosize CeO_{2-x} Nanocrystalline Particles. *Appl. Surf. Sci.* **1999**, *152*, 53–56. [[CrossRef](#)]
42. Aschauer, U.; Pfenninger, R.; Selbach, S.M.; Grande, T.; Spaldin, N.A. Strain-Controlled Oxygen Vacancy Formation and Ordering in CaMnO₃. *Phys. Rev. B* **2013**, *88*, 054111. [[CrossRef](#)]
43. Quantum Confinement Effects in Semiconductors. In *Applied Nanophotonics*; Cambridge University Press: Cambridge, UK, 2018; pp. 52–91.
44. Li, P.; Chen, X.; Li, Y.; Schwank, J.W. A Review on Oxygen Storage Capacity of CeO₂-Based Materials: Influence Factors, Measurement Techniques, and Applications in Reactions Related to Catalytic Automotive Emissions Control. *Catal. Today* **2019**, *327*, 90–115. [[CrossRef](#)]
45. Zhao, G.; Yang, F.; Chen, Z.; Liu, Q.; Ji, Y.; Zhang, Y.; Niu, Z.; Mao, J.; Bao, X.; Hu, P.; et al. Metal/Oxide Interfacial Effects on the Selective Oxidation of Primary Alcohols. *Nat. Commun.* **2017**, *8*, 14039. [[CrossRef](#)] [[PubMed](#)]
46. Xu, Z.C.; Park, E.D. Gas-Phase Selective Oxidation of Methane into Methane Oxygenates. *Catalysts* **2022**, *12*, 314. [[CrossRef](#)]
47. Karakaya, C.; Zhu, H.; Loebick, C.; Weissman, J.G.; Kee, R.J. A Detailed Reaction Mechanism for Oxidative Coupling of Methane over Mn/Na₂WO₄/SiO₂ Catalyst for Non-Isothermal Conditions. *Catal. Today* **2018**, *312*, 10–22. [[CrossRef](#)]
48. Postma, R.S.; Mendes, P.S.F.; Pirro, L.; Banerjee, A.; Thybaut, J.W.; Lefferts, L. Modelling of the Catalytic Initiation of Methane Coupling under Non-Oxidative Conditions. *Chem. Eng. J.* **2023**, *454*, 140273. [[CrossRef](#)]
49. Dummer, N.F.; Willock, D.J.; He, Q.; Howard, M.J.; Lewis, R.J.; Qi, G.; Taylor, S.H.; Xu, J.; Bethell, D.; Kiely, C.J.; et al. Methane Oxidation to Methanol. *Chem. Rev.* **2023**, *123*, 6359–6411. [[CrossRef](#)] [[PubMed](#)]
50. Deng, J.; Chen, P.; Xia, S.; Zheng, M.; Song, D.; Lin, Y.; Liu, A.; Wang, X.; Zhao, K.; Zheng, A. Advances in Oxidative Coupling of Methane. *Atmosphere* **2023**, *14*, 1538. [[CrossRef](#)]
51. Alkathiri, R.; Alshamrani, A.; Wazeer, I.; Boumaza, M.; Hadj-Kali, M.K. Optimization of the Oxidative Coupling of Methane Process for Ethylene Production. *Processes* **2022**, *10*, 1085. [[CrossRef](#)]

52. Zhang, T. Recent Advances in Heterogeneous Catalysis for the Nonoxidative Conversion of Methane. *Chem. Sci.* **2021**, *12*, 12529–12545. [[CrossRef](#)]
53. Sun, L.; Wang, Y.; Guan, N.; Li, L. Methane Activation and Utilization: Current Status and Future Challenges. *Energy Technol.* **2020**, *8*, 1900826. [[CrossRef](#)]
54. Zhao, G.; Drewery, M.; Mackie, J.; Oliver, T.; Kennedy, E.M.; Stockenhuber, M. The Catalyzed Conversion of Methane to Value-Added Products. *Energy Technol.* **2020**, *8*, 1900665. [[CrossRef](#)]
55. Wang, J.; Rao, Z.; Huang, Z.; Chen, Y.; Wang, F.; Zhou, Y. Recent Progress of Metal-Oxide-Based Catalysts for Non-Oxidative Coupling of Methane to Ethane and Hydrogen. *Catalysts* **2023**, *13*, 719. [[CrossRef](#)]
56. Ogawa, Y.; Xu, Y.; Zhang, Z.; Ma, H.; Yamamoto, Y. Development of Catalysts for Direct Non-Oxidative Methane Aromatization. *Resour. Chem. Mater.* **2022**, *1*, 80–92. [[CrossRef](#)]
57. Chen, Y.; Mu, X.; Luo, X.; Shi, K.; Yang, G.; Wu, T. Catalytic Conversion of Methane at Low Temperatures: A Critical Review. *Energy Technol.* **2020**, *8*, 1900750. [[CrossRef](#)]
58. Konnov, S.V. Direct Non-Oxidative Conversion of Methane over Metal-Containing Zeolites: Main Strategies for Shifting the Thermodynamic Equilibrium (A Review). *Pet. Chem.* **2022**, *62*, 280–290. [[CrossRef](#)]
59. Kang, J.; Park, E.D. Liquid-Phase Selective Oxidation of Methane to Methane Oxygenates. *Catalysts* **2024**, *14*, 167. [[CrossRef](#)]
60. Li, D.; Xu, R.; Gu, Z.; Zhu, X.; Qing, S.; Li, K. Chemical-Looping Conversion of Methane: A Review. *Energy Technol.* **2020**, *8*, 1900925. [[CrossRef](#)]
61. Wu, L.; Fan, W.; Wang, X.; Lin, H.; Tao, J.; Liu, Y.; Deng, J.; Jing, L.; Dai, H. Methane Oxidation over the Zeolites-Based Catalysts. *Catalysts* **2023**, *13*, 604. [[CrossRef](#)]
62. Kumar, P.; Al-Attas, T.A.; Hu, J.; Kibria, M.G. Single Atom Catalysts for Selective Methane Oxidation to Oxygenates. *ACS Nano* **2022**, *16*, 8557–8618. [[CrossRef](#)]
63. Anggoro, D.D.; Chamdani, F.T.; Buchori, L. One Step Catalytic Oxidation Process of Methane to Methanol at Low Reaction Temperature: A Brief Review. *IOP Conf. Ser. Mater. Sci. Eng.* **2021**, *1053*, 012056. [[CrossRef](#)]
64. Newton, M.A.; Knorpp, A.J.; Sushkevich, V.L.; Palagin, D.; van Bokhoven, J.A. Active Sites and Mechanisms in the Direct Conversion of Methane to Methanol Using Cu in Zeolitic Hosts: A Critical Examination. *Chem. Soc. Rev.* **2020**, *49*, 1449–1486. [[CrossRef](#)]
65. Shi, Y.; Liu, S.; Liu, Y.; Huang, W.; Guan, G.; Zuo, Z. Quasicatalytic and Catalytic Selective Oxidation of Methane to Methanol over Solid Materials: A Review on the Roles of Water. *Catal. Rev.* **2020**, *62*, 313–345. [[CrossRef](#)]
66. Sharma, R.; Poelman, H.; Marin, G.B.; Galvita, V.V. Approaches for Selective Oxidation of Methane to Methanol. *Catalysts* **2020**, *10*, 194. [[CrossRef](#)]
67. Zhu, Z.; Guo, W.; Zhang, Y.; Pan, C.; Xu, J.; Zhu, Y.; Lou, Y. Research Progress on Methane Conversion Coupling Photocatalysis and Thermocatalysis. *Carbon. Energy* **2021**, *3*, 519–540. [[CrossRef](#)]
68. Cruchade, H.; Medeiros-Costa, I.C.; Nesterenko, N.; Gilson, J.-P.; Pinard, L.; Beuque, A.; Mintova, S. Catalytic Routes for Direct Methane Conversion to Hydrocarbons and Hydrogen: Current State and Opportunities. *ACS Catal.* **2022**, *12*, 14533–14558. [[CrossRef](#)]
69. Arinaga, A.M.; Ziegelski, M.C.; Marks, T.J. Alternative Oxidants for the Catalytic Oxidative Coupling of Methane. *Angew. Chem. Int. Ed.* **2021**, *60*, 10502–10515. [[CrossRef](#)]
70. Liu, J.; Yue, J.; Lv, M.; Wang, F.; Cui, Y.; Zhang, Z.; Xu, G. From Fundamentals to Chemical Engineering on Oxidative Coupling of Methane for Ethylene Production: A Review. *Carbon. Resour. Convers.* **2022**, *5*, 1–14. [[CrossRef](#)]
71. Kim, K.-J.; Kim, K.Y.; Rhim, G.B.; Youn, M.H.; Lee, Y.-L.; Chun, D.H.; Roh, H.-S. Nano-Catalysts for Gas to Liquids: A Concise Review. *Chem. Eng. J.* **2023**, *468*, 143632. [[CrossRef](#)]
72. Ma, X.; Li, Y.; Huang, X.; Feng, T.; Mu, M. Sorption-Enhanced Reaction Process Using Advanced Ca-Based Sorbents for Low-Carbon Hydrogen Production. *Process Saf. Environ. Prot.* **2021**, *155*, 325–342. [[CrossRef](#)]
73. Chen, L.; Qi, Z.; Zhang, S.; Su, J.; Somorjai, G.A. Catalytic Hydrogen Production from Methane: A Review on Recent Progress and Prospect. *Catalysts* **2020**, *10*, 858. [[CrossRef](#)]
74. Torimoto, M.; Sekine, Y. Effects of Alloying for Steam or Dry Reforming of Methane: A Review of Recent Studies. *Catal. Sci. Technol.* **2022**, *12*, 3387–3411. [[CrossRef](#)]
75. Meloni, E.; Martino, M.; Palma, V. A Short Review on Ni Based Catalysts and Related Engineering Issues for Methane Steam Reforming. *Catalysts* **2020**, *10*, 352. [[CrossRef](#)]
76. Jagadeesh, P.; Varun, Y.; Himajaa Reddy, B.; Sreedhar, I.; Singh, S.A. A Short Review on Recent Advancements of Dry Reforming of Methane (DRM) over Pyrochlores. *Mater. Today Proc.* **2023**, *72*, 361–369. [[CrossRef](#)]
77. Xu, Z.; Park, E.D. Recent Advances in Coke Management for Dry Reforming of Methane over Ni-Based Catalysts. *Catalysts* **2024**, *14*, 176. [[CrossRef](#)]
78. Abdulrasheed, A.; Jalil, A.A.; Gambo, Y.; Ibrahim, M.; Hambali, H.U.; Hamid, M.Y.S. A Review on Catalyst Development for Dry Reforming of Methane to Syngas: Recent Advances. *Renew. Sustain. Energy Rev.* **2019**, *108*, 175–193. [[CrossRef](#)]
79. Bhattar, S.; Abedin, M.A.; Kanitkar, S.; Spivey, J.J. A Review on Dry Reforming of Methane over Perovskite Derived Catalysts. *Catal. Today* **2021**, *365*, 2–23. [[CrossRef](#)]
80. Yentekakis, I.V.; Panagiotopoulou, P.; Artemakis, G. A Review of Recent Efforts to Promote Dry Reforming of Methane (DRM) to Syngas Production via Bimetallic Catalyst Formulations. *Appl. Catal. B* **2021**, *296*, 120210. [[CrossRef](#)]

81. Teh, L.P.; Setiabudi, H.D.; Timmiati, S.N.; Aziz, M.A.A.; Annuar, N.H.R.; Ruslan, N.N. Recent Progress in Ceria-Based Catalysts for the Dry Reforming of Methane: A Review. *Chem. Eng. Sci.* **2021**, *242*, 116606. [[CrossRef](#)]
82. Torrez-Herrera, J.J.; Korili, S.A.; Gil, A. Recent Progress in the Application of Ni-Based Catalysts for the Dry Reforming of Methane. *Catal. Rev.* **2023**, *65*, 1300–1357. [[CrossRef](#)]
83. Hussien, A.G.S.; Polychronopoulou, K. A Review on the Different Aspects and Challenges of the Dry Reforming of Methane (DRM) Reaction. *Nanomaterials* **2022**, *12*, 3400. [[CrossRef](#)]
84. Sher Shah, M.S.A.; Oh, C.; Park, H.; Hwang, Y.J.; Ma, M.; Park, J.H. Catalytic Oxidation of Methane to Oxygenated Products: Recent Advancements and Prospects for Electrocatalytic and Photocatalytic Conversion at Low Temperatures. *Adv. Sci.* **2020**, *7*, 2001946. [[CrossRef](#)]
85. Wang, Q.; Kan, M.; Han, Q.; Zheng, G. Electrochemical Methane Conversion. *Small Struct.* **2021**, *2*, 2100037. [[CrossRef](#)]
86. Xie, S.; Lin, S.; Zhang, Q.; Tian, Z.; Wang, Y. Selective Electrocatalytic Conversion of Methane to Fuels and Chemicals. *J. Energy Chem.* **2018**, *27*, 1629–1636. [[CrossRef](#)]
87. Abdelkader Mohamed, A.G.; Zahra Naqviab, S.A.; Wang, Y. Advances and Fundamental Understanding of Electrocatalytic Methane Oxidation. *ChemCatChem* **2021**, *13*, 787–805. [[CrossRef](#)]
88. Liu, F.; Yan, Y.; Chen, G.; Wang, D. Recent Advances in Ambient Electrochemical Methane Conversion to Oxygenates Using Metal Oxide Electrocatalysts. *Green. Chem.* **2024**, *26*, 655–677. [[CrossRef](#)]
89. Kishore, M.R.A.; Lee, S.; Yoo, J.S. Fundamental Limitation in Electrochemical Methane Oxidation to Alcohol: A Review and Theoretical Perspective on Overcoming It. *Adv. Sci.* **2023**, *10*, 2301912. [[CrossRef](#)]
90. Yan, L.; Jiang, L.; Qian, C.; Zhou, S. Electrocatalytic Conversion of Methane: Recent Progress and Future Prospects. *Energy Rev.* **2024**, *3*, 100065. [[CrossRef](#)]
91. Shi, T.; Sridhar, D.; Zeng, L.; Chen, A. Recent Advances in Catalyst Design for the Electrochemical and Photoelectrochemical Conversion of Methane to Value-Added Products. *Electrochem. Commun* **2022**, *135*, 107220. [[CrossRef](#)]
92. Jiang, H.; Zhang, L.; Han, Z.; Tang, Y.; Sun, Y.; Wan, P.; Chen, Y.; Argyle, M.D.; Fan, M. Direct Conversion of Methane to Methanol by Electrochemical Methods. *Green. Energy Environ.* **2022**, *7*, 1132–1142. [[CrossRef](#)]
93. Wang, P.; Shi, R.; Zhao, J.; Zhang, T. Photodriven Methane Conversion on Transition Metal Oxide Catalyst: Recent Progress and Prospects. *Adv. Sci.* **2024**, *11*, 2305471. [[CrossRef](#)]
94. Lin, X.-Y.; Li, J.-Y.; Qi, M.-Y.; Tang, Z.-R.; Xu, Y.-J. Methane Conversion over Artificial Photocatalysts. *Catal. Commun.* **2021**, *159*, 106346. [[CrossRef](#)]
95. Li, Q.; Ouyang, Y.; Li, H.; Wang, L.; Zeng, J. Photocatalytic Conversion of Methane: Recent Advancements and Prospects. *Angew. Chem.* **2022**, *134*, 2108069. [[CrossRef](#)]
96. Wu, X.; Zhang, H.; Xie, S.; Wang, Y. Photocatalytic Conversion of Methane: Catalytically Active Sites and Species. *Chem. Catal.* **2023**, *3*, 100437. [[CrossRef](#)]
97. Xu, Y.; Chen, E.; Tang, J. Photocatalytic Methane Conversion to High-Value Chemicals. *Carbon. Future* **2024**, *1*, 9200004. [[CrossRef](#)]
98. Jiang, Y.; Li, S.; Fan, Y.; Tang, Z. Best Practices for Experiments and Reports in Photocatalytic Methane Conversion. *Angew. Chem.* **2024**, *4*, 2404658. [[CrossRef](#)]
99. Jiang, Y.; Fan, Y.; Li, S.; Tang, Z. Photocatalytic Methane Conversion: Insight into the Mechanism of C(Sp³)–H Bond Activation. *CCS Chem.* **2023**, *5*, 30–54. [[CrossRef](#)]
100. Sader, S.; Miliordos, E. Methane to Methanol Conversion Facilitated by Anionic Transition Metal Centers: The Case of Fe, Ni, Pd, and Pt. *J. Phys. Chem. A* **2021**, *125*, 2364–2373. [[CrossRef](#)]
101. Vali, S.A.; Markeb, A.A.; Moral-Vico, J.; Font, X.; Sánchez, A. Recent Advances in the Catalytic Conversion of Methane to Methanol: From the Challenges of Traditional Catalysts to the Use of Nanomaterials and Metal–Organic Frameworks. *Nanomaterials* **2023**, *13*, 2754. [[CrossRef](#)]
102. Bobadilla, L.F.; Garcilaso, V.; Centeno, M.A.; Odriozola, J.A. Monitoring the Reaction Mechanism in Model Biogas Reforming by In Situ Transient and Steady-State DRIFTS Measurements. *ChemSusChem* **2017**, *10*, 1193–1201. [[CrossRef](#)]
103. Blaylock, D.W.; Ogura, T.; Green, W.H.; Beran, G.J.O. Computational Investigation of Thermochemistry and Kinetics of Steam Methane Reforming on Ni(111) under Realistic Conditions. *J. Phys. Chem. C* **2009**, *113*, 4898–4908. [[CrossRef](#)]
104. González-Castaño, M.; Dorneanu, B.; Arellano-García, H. The Reverse Water Gas Shift Reaction: A Process Systems Engineering Perspective. *React. Chem. Eng.* **2021**, *6*, 954–976. [[CrossRef](#)]
105. Chen, L.; Pilot, I.A.W.; Hensen, E.J.M. Elucidation of the Reverse Water–Gas Shift Reaction Mechanism over an Isolated Ru Atom on CeO₂(111). *J. Phys. Chem. C* **2023**, *127*, 20314–20324. [[CrossRef](#)]
106. Sun, Y.; Zhang, G.; Cheng, H.; Liu, J.; Li, G. Kinetics and Mechanistic Studies of Methane Dry Reforming over Ca Promoted 1Co–1Ce/AC-N Catalyst. *Int. J. Hydrogen Energy* **2021**, *46*, 531–542. [[CrossRef](#)]
107. Yu, Y.; Ji, P.; Zhang, W.; Yang, K.; Zhang, M. Theoretical Study Coupling DFT Calculations and KMC Simulation of CO Methanation on Ni(111) and Ni₃Fe(111). *New J. Chem.* **2023**, *47*, 17923–17936. [[CrossRef](#)]
108. Zhang, Q.; Bown, M.; Pastor-Pérez, L.; Duyar, M.S.; Reina, T.R. CO₂ Conversion via Reverse Water Gas Shift Reaction Using Fully Selective Mo–P Multicomponent Catalysts. *Ind. Eng. Chem. Res.* **2022**, *61*, 12857–12865. [[CrossRef](#)] [[PubMed](#)]
109. Santos, M.F.; Bresciani, A.E.; Ferreira, N.L.; Bassani, G.S.; Alves, R.M.B. Carbon Dioxide Conversion via Reverse Water-Gas Shift Reaction: Reactor Design. *J. Environ. Manag.* **2023**, *345*, 118822. [[CrossRef](#)] [[PubMed](#)]

110. Ma, M.; Jin, B.J.; Li, P.; Jung, M.S.; Kim, J.I.; Cho, Y.; Kim, S.; Moon, J.H.; Park, J.H. Ultrahigh Electrocatalytic Conversion of Methane at Room Temperature. *Adv. Sci.* **2017**, *4*, 1700379. [[CrossRef](#)]
111. Özdemir, H.; Çiftçiöğlü, E.; Faruk Öksüzömer, M.A. Lanthanum Based Catalysts for Oxidative Coupling of Methane: Effect of Morphology and Structure. *Chem. Eng. Sci.* **2023**, *270*, 118520. [[CrossRef](#)]
112. Bresciani, L.; Stülpe, S. Electrochemical Deposition of Pt and Pd on TiO₂ Nanotubes for Application in the Photoelectrocatalytic Conversion of Biomethane and Biogas for Hydrogen Generation. *Electrocatalysis* **2024**, *15*, 70–86. [[CrossRef](#)]
113. Özdemir, H. Detailed Investigation of Sm₂O₃ Catalysts with Different Morphologies for Oxidative Coupling of Methane. *ChemistrySelect* **2021**, *6*, 7999–8006. [[CrossRef](#)]
114. Kim, I.; Lee, G.; Na, H.B.; Ha, J.-M.; Jung, J.C. Selective Oxygen Species for the Oxidative Coupling of Methane. *Mol. Catal.* **2017**, *435*, 13–23. [[CrossRef](#)]
115. Premachandra, D.; Heagy, M.D. Morphology-Controlled WO₃ for the Photocatalytic Oxidation of Methane to Methanol in Mild Conditions. *Methane* **2023**, *2*, 103–112. [[CrossRef](#)]
116. Chen, J.; Pham, H.N.; Mon, T.; Toops, T.J.; Datye, A.K.; Li, Z.; Kyriakidou, E.A. Ni/CeO₂ Nanocatalysts with Optimized CeO₂ Support Morphologies for CH₄ Oxidation. *ACS Appl. Nano Mater.* **2023**, *6*, 4544–4553. [[CrossRef](#)]
117. Rodrigues, T.S.; e Silva, F.A.; Candido, E.G.; da Silva, A.G.M.; Geonmonond, R.d.S.; Camargo, P.H.C.; Linardi, M.; Fonseca, F.C. Ethanol Steam Reforming: Understanding Changes in the Activity and Stability of Rh/MxO_y Catalysts as Function of the Support. *J. Mater. Sci.* **2019**, *54*, 11400–11416. [[CrossRef](#)]
118. Ma, J.; Tan, X.; Zhang, Q.; Wang, Y.; Zhang, J.; Wang, L. Exploring the Size Effect of Pt Nanoparticles on the Photocatalytic Nonoxidative Coupling of Methane. *ACS Catal.* **2021**, *11*, 3352–3360. [[CrossRef](#)]
119. Kiss, J.; Kukovecz, Á.; Kónya, Z. Beyond Nanoparticles: The Role of Sub-Nanosized Metal Species in Heterogeneous Catalysis. *Catal. Lett.* **2019**, *149*, 1441–1454. [[CrossRef](#)]
120. Zhu, M.; Aikens, C.M.; Hollander, F.J.; Schatz, G.C.; Jin, R. Correlating the Crystal Structure of A Thiol-Protected Au₂₅ Cluster and Optical Properties. *J. Am. Chem. Soc.* **2008**, *130*, 5883–5885. [[CrossRef](#)] [[PubMed](#)]
121. Wu, Z.; Jiang, D.; Mann, A.K.P.; Mullins, D.R.; Qiao, Z.-A.; Allard, L.F.; Zeng, C.; Jin, R.; Overbury, S.H. Thiolate Ligands as a Double-Edged Sword for CO Oxidation on CeO₂ Supported Au₂₅ (SCH₂CH₂Ph)₁₈ Nanoclusters. *J. Am. Chem. Soc.* **2014**, *136*, 6111–6122. [[CrossRef](#)]
122. László, B.; Baán, K.; Varga, E.; Oszkó, A.; Erdőhelyi, A.; Kónya, Z.; Kiss, J. Photo-Induced Reactions in the CO₂-Methane System on Titanate Nanotubes Modified with Au and Rh Nanoparticles. *Appl. Catal. B* **2016**, *199*, 473–484. [[CrossRef](#)]
123. Gualteros, J.A.D.; Garcia, M.A.S.; da Silva, A.G.M.; Rodrigues, T.S.; Cândido, E.G.; e Silva, F.A.; Fonseca, F.C.; Quiroz, J.; de Oliveira, D.C.; de Torresi, S.I.C.; et al. Synthesis of Highly Dispersed Gold Nanoparticles on Al₂O₃, SiO₂, and TiO₂ for the Solvent-Free Oxidation of Benzyl Alcohol under Low Metal Loadings. *J. Mater. Sci.* **2019**, *54*, 238–251. [[CrossRef](#)]
124. Subramanian, V.; Wolf, E.E.; Kamat, P.V. Catalysis with TiO₂/Gold Nanocomposites. Effect of Metal Particle Size on the Fermi Level Equilibration. *J. Am. Chem. Soc.* **2004**, *126*, 4943–4950. [[CrossRef](#)] [[PubMed](#)]
125. Ismail, A.A.; Bahnemann, D.W.; Bannat, I.; Wark, M. Gold Nanoparticles on Mesoporous Interparticle Networks of Titanium Dioxide Nanocrystals for Enhanced Photonic Efficiencies. *J. Phys. Chem. C* **2009**, *113*, 7429–7435. [[CrossRef](#)]
126. Sheng, K.; Luan, D.; Jiang, H.; Zeng, F.; Wei, B.; Pang, F.; Ge, J. Ni_xCo_y Nanocatalyst Supported by ZrO₂ Hollow Sphere for Dry Reforming of Methane: Synergetic Catalysis by Ni and Co in Alloy. *ACS Appl. Mater. Interfaces* **2019**, *11*, 24078–24087. [[CrossRef](#)]
127. Chen, J.; Wang, S.; Peres, L.; Collière, V.; Philippot, K.; Lecante, P.; Chen, Y.; Yan, N. Oxidation of Methane to Methanol over Pd@Pt Nanoparticles under Mild Conditions in Water. *Catal. Sci. Technol.* **2021**, *11*, 3493–3500. [[CrossRef](#)]
128. Wang, Y.; Xiao, L.; Qi, Y.; Yang, J.; Zhu, Y.-A.; Chen, D. Insight into Size- and Metal-Dependent Activity and the Mechanism for Steam Methane Re-Forming in Nanocatalysis. *J. Phys. Chem. C* **2020**, *124*, 2501–2512. [[CrossRef](#)]
129. Wang, W.-Y.; Liu, J.-H.; Lv, C.-Q.; Ren, R.-R.; Wang, G.-C. Dry Reforming of Methane on Ni(1 1 1) Surface with Different Mo Doping Ratio: DFT-Assisted Microkinetic Study. *Appl. Surf. Sci.* **2022**, *581*, 152310. [[CrossRef](#)]
130. Wang, Y.-X.; Zhang, H.-L.; An, P.; Wu, H.-S.; Jia, J.-F. Effect of Potassium on Methanol Steam Reforming on the Cu(111) and Cu(110) Surfaces: A DFT Study. *J. Phys. Chem. C* **2021**, *125*, 20905–20918. [[CrossRef](#)]
131. Yadavalli, S.S.; Jones, G.; Stamatakis, M. DFT Benchmark Studies on Representative Species and Poisons of Methane Steam Reforming on Ni(111). *Phys. Chem. Chem. Phys.* **2021**, *23*, 15601–15612. [[CrossRef](#)]
132. Xu, L.; Papanikolaou, K.G.; Lechner, B.A.J.; Je, L.; Somorjai, G.A.; Salmeron, M.; Mavrikakis, M. Formation of Active Sites on Transition Metals through Reaction-Driven Migration of Surface Atoms. *Science* **2023**, *380*, 70–76. [[CrossRef](#)]
133. Tsuji, Y.; Yoshida, M.; Yoshizawa, K.; Kamachi, T. Concepts of Computational Approach to Explore Heterogeneous Catalysts for Direct Methane Conversion. *ChemCatChem* **2023**, *15*, 2201488. [[CrossRef](#)]

Disclaimer/Publisher's Note: The statements, opinions and data contained in all publications are solely those of the individual author(s) and contributor(s) and not of MDPI and/or the editor(s). MDPI and/or the editor(s) disclaim responsibility for any injury to people or property resulting from any ideas, methods, instructions or products referred to in the content.